QUANTUM OPTICAL PHENOMENA IN PHOTONIC CRYSTALS - FROM

QUANTUM SQUEEZING TO QUANTUM ENTANGLEMENT

by

RAY-KUANG LEE

A DISSERTATION

Presented to the Department of Photonics
and the Institute of Electro-Optical Engineering, National Chiao-Tung University,
Hsinchu, Taiwan
in partial fulfillment of the requirements
for the degree of
Doctor of Philosophy
in Electrical Engineering and Computer Science

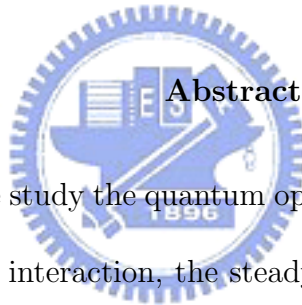Hsinchu, Taiwan, December 2004

**QUANTUM OPTICAL PHENOMENA IN PHOTONIC CRYSTALS -
FROM QUANTUM SQUEEZING TO QUANTUM ENTANGLEMENT**

Student: Ray-Kuang Lee   Advisor: Dr. Yinchieh Lai

Department of Photonics and the Institute of Electro-Optical Engineering

National Chiao-Tung University

Abstract

In this dissertation we study the quantum optical phenomena in photonic crystals. In the part of atom-light interaction, the steady state fluorescence spectra of a two-level atom embedded in a three-dimensional photonic bandgap crystal are predicted to get squeezed in the in-phase quadrature spectra. In the part of nonlinear photonic crystals, we use the back-propagation method to study the quantum fluctuations of optical Bragg solitons propagating in nonlinear fiber Bragg gratings and matter-wave gap solitons in optical lattices. Finally, new schemes for generating continuous-variable entangled states through continuous interaction of two solitons are proposed to produce entangled optical sources for quantum communication and computation.

CURRICULUM VITA

NAME OF AUTHOR :   Ray-Kuang Lee

PLACE OF BIRTH :   Keelung, Taiwan

DATE OF BIRTH :   October 24, 1974

CONTACT :   rklee.eo89g@nctu.edu.tw

DEGREES OF EDUCATION :

> Doctor of Philosophy in EECS,
> > National Chiao-Tung University, Sep. 2000 - Dec. 2004.
> Master of Science in EECS,
> > National Chiao-Tung University, Sep. 1997 - Jun. 1999.
> Bachelor of Engineering in EECS,
> > National Taiwan University, Sep. 1993 - Jun. 1997.

AREAS OF SPECIAL INTEREST :

> Quantum optics, Nonlinear Physics, and Fiber Lasers.

PROFESSIONAL EXPERIENCE :

> Visiting Student at Nonlinear Physics Centre (Head: Yuri S. Kivshar),
> > The Australian National University, Apr. 2004 - Dec. 2004.
> Assistant Research Scientist,
> > National Laboratory, Oct. 1999 - Apr. 2004.

AWARDS AND HONORS :

- Award for Graduate Students Study Abroad Program, supported by National Science Council, Taiwan, 2004.

- Student Paper Award, "Classical-interference analog of quantum fluctuations for bound-soliton pairs in fiber lasers," in Optics and Photonics Taiwan 2004.

PUBLICATION LIST:

Refereed Journal Papers

1. <u>Ray-Kuang Lee</u> and Yinchieh Lai, "Amplitude-squeezed fiber-Bragg-grating solitons," *Phys. Rev. A* **69**, 021801(R) (2004); also as part of *Virtual Journal of Nanoscale Science & Technology* **9**, Issue 8 (2004).

2. <u>Ray-Kuang Lee</u> and Yinchieh Lai, and Boris A. Malomed, "Quantum Fluctuations around Bistable Solitons in the Cubic-Quintic nonlinear Schrödinger equation," *J. Opt. B* **6**, 367 (2004).

3. <u>Ray-Kuang Lee</u> and Yinchieh Lai, "Quantum theory of fiber Bragg grating solitons," *J. Opt. B* **6**, S638 (2004).

4. <u>Ray-Kuang Lee</u> and Yinchieh Lai, "Fluorescence squeezing spectra near a photonic bandgap," *J. Opt. B* **6**, S715 (2004).

5. <u>Ray-Kuang Lee</u>, Yinchieh Lai, and Boris Malomed, "Quantum correlations in bound-soliton pairs and trains in fiber lasers," *Phys. Rev. A* **70**, xxxxxx (2004); quant-ph/0408175.

6. <u>Ray-Kuang Lee</u>, Yinchieh Lai, and Boris Malomed, "Generation of photon-number entangled soliton pairs through interactions," *Phys. Rev. A* **71**, xxxxxx (2005); quant-ph/0405138.

7. <u>Ray-Kuang Lee</u>, Elena A. Ostrovskaya, Yuri S. Kivshar, and Yinchieh Lai, "Squeezing and entanglement of matter-wave gap solitons," submitted for publication; quant-ph/0412036.

8. <u>Ray-Kuang Lee</u>, Yinchieh Lai, and Boris A. Malomed, "Classical-interference analog of quantum fluctuations for bound-state soliton pairs," submitted for publication.

9. <u>Ray-Kuang Lee</u>, and Yinchieh Lai, Yuri S. Kivshar, "Quantum correlations in the soliton collisions," submitted for publication.

Proceedings of Conference

1. Ray-Kuang Lee and Yinchieh Lai, "Resonance Fluorescence Spectrum near Photonic Bandgap," *SPIE Photonics West 2003*, 5000-20, San Jose, California, USA, 25-31 January (2003).

2. Ray-Kuang Lee and Yinchieh Lai, "Resonance Fluorescence Spectrum in a Two-Band Photonic Bandgap Crystal," *SPIE First International Symposium on Fluctuation and Noise*, 5111-27, Santa Fe, New Mexico, USA, 1-4 June (2003).

3. Ray-Kuang Lee and Yinchieh Lai, "Steady-state fluorescence spectrum of a two-level atom in three-dimensional photonic crystals," *CLEO/Pacific-Rrm 2003*, P0405, Taipei, Taiwan 15-19 December (2003).

4. Ray-Kuang Lee and Yinchieh Lai, "Quantum theory of Bragg solitons: Linearized approach," *CLEO/Pacific-Rim 2003*, P0401, Taipei, Taiwan, 15-19 December (2003).

5. Ray-Kuang Lee and Yinchieh Lai, "Quantum Theory of Fiber Bragg Grating Solitons," *Optics and Photonics Taiwan 2003*, PD1-4, National Taipei University of Technology, Taipei, Taiwan, 25-26 December (2003).

6. Ray-Kuang Lee and Yinchieh Lai, "Quantum fluctuations of Bragg grating solitons in apodized fiber gratings," *Annual Meetings of The Physical Society of Taiwan*, PE-57, National Tsing Hua University, Hsinchu, Taiwan, 9-11 February (2004).

7. Ray-Kuang Lee, Yinchieh Lai, and Boris Malomed, "Squeezing of Bi-solitons in Cubic-Quintic Schrödinger Equations," *OSA Nonlinear Guided Waves and Their Applications*, MC-5, Toronto, Canada, 28-31 March (2004).

8. Ray-Kuang Lee and Yinchieh Lai, "Interaction induced photon-number entangled temporal soliton pairs," *OSA Nonlinear Optics*, FA3, Waikoloa, Hawaii, USA, 2-6 August (2004).

9. Ray-Kuang Lee and Yinchieh Lai, "Classical-interference analog of quantum fluctuations for bound-soliton pairs in fiber lasers," *Optics and Photonics Taiwan 2004*, C-SA-IV2-8, National Central University, Taoyuan, Taiwan, 18-19 December (2004).

Talks in Seminar/Workshop and Others

1. Ray-Kuang Lee, "Quantum Information with Optical Systems," *Quantum Information Workshop*, The Industrial Technology Research Institute (ITRI), Hsinchu, Taiwan, 1 October (2003).

2. Yinchieh Lai, and Ray-Kuang Lee, "Quantum Optical Effects in Photonic Crystals," *Workshop on Advanced Photonic-Crystal Devices*, National Taiwan Normal University, Taipei, Taiwan, 18-19 October (2003).

3. Ray-Kuang Lee, "Quantum Theory of Bragg Solitons," *Department Seminar*, Institute of Electro-Optical Engineering, National Chiao-Tung University, Hsinchu, Taiwan, 12 December (2003).

4. Ray-Kuang Lee and Yinchieh Lai, "Quantum Optical Effects in Photonic Crystals," *Optical Engineering Journal* (in Traditional Chinese), **83**, 48 (2003).

5. Ray-Kuang Lee, "Quantum Noise Squeezing and Quantum Correlations of Optical Solitons," *Department Seminar*, Nonlinear Physics Centre, Research School of Physical Sciences and Engineering, The Australian National University, Canberra, Australia, 19 May (2004).

6. Ray-Kuang Lee and Yinchieh Lai, "Fluorescence Spectra of a Two-Level Atom Embedded in a Three-Dimensional Photonic Crystal," quant-ph/0308106 (un-published paper).

TABLE OF CONTENTS

List of Figures

CHAPTER 1

Introduction

1.1. Motivation

The study of Photonic Crystals (PhCs), which is the electromagnetic analog of semiconductor crystals, can be tracked back to Lord Rayleigh in 1887 when he identified the fact that the crystalline mineral with periodic "twinning" planes has a narrow band gap prohibiting light propagation. This angle-dependent band gap effect is due to the multilayer thin film structure in one-dimension, similar to many other iridescent colors in nature, such as butterfly wings, abalone shells, and Australian opals in Fig. 1.1 [1].

Extending the idea to two and three dimensions, Yablonovitch [1] and John [2] in 1987 introduced the new kind of man-made crystals, called Electromagnetic Crystals or Photonic Bandgap Crystals, which also stirred the imagination toward compact photonic integrated circuits. In recent years, with the advance of new fabrication technologies, it has become more feasible to actually utilize higher dimensional periodic dielectric structures (or especially the photonic bandgap crystals) for modifying the properties of the photon states as well as the properties of the spontaneous emis-

---

[1]Source: www.lostseaopals.com.au

FIGURE 1.1: Due to the periodic structures in the surface, Australian Opal is the only gemstone that holds all colours of the spectrum. Every opal has a unique play of colour and pattern.

sion. Generally, photonic crystals possess photonic band gaps where light cannot propagate through the structure within a certain range of wavelengths (the bandgap) due to the lack of available photon states. The introduction of defects in the photonic crystals (analogous to electronic dopants) can give rise to localized electromagnetic states, which can act as waveguides and point-like cavities. The photonic crystals thus can provide novel possibilities for the control of electromagnetic phenomena.

With the existence of a forbidden electromagnetic bandgap, photonic crystals can be used to not only control the flow of lights but also their quantum optical properties. It has been well known that the spontaneous emission from an excited atom can be modified by the electromagnetic reservoir that surrounds the atom (the Purcell effect [3]). In contrast to the free space case where the distribution of the photon density states is more uniform, the impacts of such a non-uniform photon state distribution upon the characteristics of the resonance fluorescence from a two-level atom with its

emission wavelength near the bandgap are investigated in **Chapter 2**. Such a non-uniform distribution of the photon density of states has been investigated by many authors and has provided a new and experimentally feasible platform for investigating photon-atom interaction. Many new quantum optical phenomena [4, 5, 6, 7, 8, 9] have been theoretically discovered in the presence of the bandgap. However, all of the above studies only focused on the transient behavior of the atom-photon interactions and to the best of our knowledge there is still no theoretical treatment on calculating the steady-state fluorescence spectra in PhCs. To investigate the steady-state problem of photon-atom interaction in PhCs, we use a new approach to treat the photon states of the photonic crystal as the background reservoir and introduce non-Markovian noise operators caused by the non-uniform DOS distribution near the band edge. Based on the theory, we show that the spectral shape of the fluorescence intensity spectra vary with the wavelength offset between the atomic transition wavelength and the bandedge. More interestingly, squeezing phenomena are found to be present in the in-phase quadrature spectra instead of the out-of-phase quadrature spectra.

In optical fibers, which are three-dimensional structures but with translational invariance along the propagation axis, one can induce one-dimensional Bragg gratings inside the fiber core by the side-illumination of the UV interference lights. The fiber Bragg gratings (FBGs) formed this way can also be viewed as a one-dimensional photonic bandgap crystal for the guiding mode of the single-mode fiber. It has been shown that a fiber Bragg grating with Kerr nonlinearity can exhibit optical soliton-like
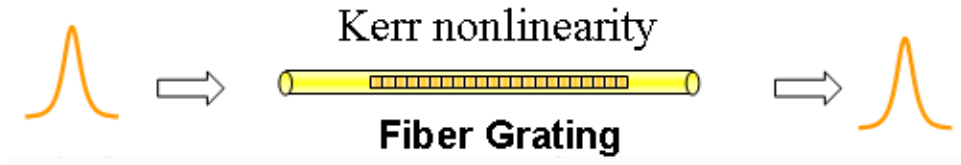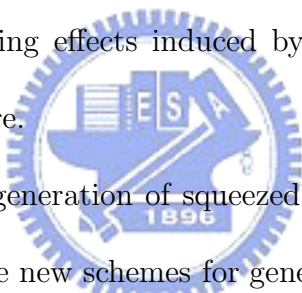
FIGURE 1.2: Illustration of a fiber Bragg grating soliton proprogating inside a optical fiber.

phenomena known as the fiber Bragg grating solitons [10]. Intuitively the fiber Bragg grating soliton can be formed if the input pulse has the suitable pulse-width and peak intensity such that the nonlinear Kerr effect is large enough to compensate the high anomalous dispersion near one of the bandedge of the FBG, see the illustration in Fig. 1.2.

From the theoretical point of view, fiber Bragg grating solitons belong to the class of bi-directional pulse propagation problems, where the quantum theory is still lack of enough consideration. In **Chapter 3**, we extend the quantum theory of nonlinear traveling wave pulses into the case of nonlinear bi-directional propagation problems and give special consideration to the quantum propagation effects of fiber Bragg grating solitons. It will be shown that the fiber Bragg grating solitons will quantum-mechanically get amplitude-squeezed after passing through the fiber grating and the squeezing ratio can be calculated theoretically. With the use of apodized FBGs, we also find that one can tailor the squeezing ratio of the FBG solitons as long as the soliton pulses evolve adiabatically.

From a broader point of view, the gap solitons, which are the localized wave-

packets in periodic structures, can also be found in the two- or three-dimensional nonlinear photonic bandgap crystals [11, 12]. The Bose-Einstein condensate (BEC) matter wave loaded into the optical lattices [13, 14, 15] is another important example, which have provided a new platform to understand the interactions between the nonlinearity and the periodicity. In **Chapter 3** we also study quantum fluctuations of matter-wave gap solitons in an optical lattice and investigate the band-gap effect on the quantum noise squeezing. We employ the soliton perturbation approach [16] to analyze the quantum fluctuations around the soliton solutions of the Gross-Pitaevskii equation with a periodic potential. Using this approach, we demonstrate enhancement of quantum noise squeezing effects induced by the evolution of gap solitons in an atomic band-gap structure.

After examining the generation of squeezed states from Bragg and gap solitons, in **Chapter 4** we propose new schemes for generating continuous-variable entangled states through *continuous interaction* of two fiber-optic solitons. In contrast to the known method for achieving an EPR pulse source by combining the two output pulse squeezed states through a beam splitter, almost perfect correlation between the photon-number fluctuations of the soliton pair can be achieved after their propagating a certain distance, if with a suitable initial separation between the two solitons. Nearly maximum photon-number entanglement in the soliton pairs can be produced in the systems including the single-polarization fiber soliton system with two time-separated solitons, the bimodal fiber soliton system with two polarizations, and the bound-state

system of gap solitons. These results offer novel possibilities to provide a favorable environment for the generation of entangled soliton pairs, which maybe the first step for developing new light sources for quantum communication and computation.

1.2.   Dissertation Organization

The thesis is organized as follows. Following the introduction part in **Chapter 1**, the fluorescence intensity and quadrature spectra from a two-level atom embedded in a photonic bandgap crystal and resonantly driven by a classical pump light are calculated in **Chapter 2**. Then we use the nonlinear coupled mode equations to describe the waves propagating in one-dimensional PhCs and study the quantum effects of optical solitons in FBGs by developing a general quantum theory of bi-directional nonlinear optical pulse propagation in **Chapter 3**. In the same chapter, we also extend the work to the matter-wave gap solitons described by the Gross-Pitaevskii equation with a periodic potential. In **Chapter 4**, new schemes for generating macroscopic (many-photon) continuous-variable entangled states by means of continuous interactions between solitons are proposed and investigated. Finally, in **Chapter 5** we briefly conclude the thesis and discuss the possible research directions that can be pursued in the future.

CHAPTER 2

Fluorescence Squeezing Spectra in 3D Photonic Crystals

2.1. Introduction

The study of fluorescence spectra from two-level atoms have been a central topic in quantum optics since the beginning era of quantum mechanics in 1930's. From the view point of light scattering, both elastic Rayleigh scattering and inelastic Raman scattering processes are involved [17] and thus the fluorescence spectra will have a triplet shape as first calculated by Mollow [18]. Theoretical calculations of the fluorescence spectra has been explored [19, 20] and also verified in experiments [21]. The squeezing phenomena in the phase-dependent fluorescence spectra of the quadrature field components were first predicted by Walls and Zoller [22] and Mandel [23]. It has been theoretically shown that the squeezing can be found in the out-of-phase quadrature component spectra under the condition that $\Omega^2 < 4\Gamma^2$ [24, 25], where Ω is the Rabi frequency and Γ is the atomic decay rate. Squeezed fluorescence spectra have also been experimentally observed in an experiment using [174]Yb atoms [26].

In recent years the atom-photon interaction in photonic crystals (PhCs) [1, 2] has been found to exhibit many interesting new phenomena such as photon-atom bound states [4], spectral splitting [5], quantum interference dark line effect [6], phase

control of spontaneous emission [7], transparency near band edge [8], and single-atom switching [9]. From the Aulter-Townes spectra for atoms coupled to a photonic bandgap structure [5] (or equivalently a frequency-depended photon density of states [27]), the modification of the spontaneous emission caused by the environment (the Purcell effect [3]) actually can be verified. However, all of the above studies only focused on the transient behavior of the atom-photon interactions and to the best of our knowledge there is still no theoretical treatment on calculating the steady-state fluorescence spectra in photonic bandgap crystals.

In the theoretical studies of fluorescence spectra for the free space case, the Markovian approximation is usually used to describe the statistical properties of the optical noises. This is a good assumption for the free space case but is not applicable for the case of photonic bandgap crystals. This is because in a photonic bandgap crystal, the distributions of the photonic density of states (DOS) are typically highly non-uniform near the bandedge. Such a property has prohibited the direct applicability of the Markovian approximation to simplify the derivation for the problem we are going to consider.

The aim of this **Chapter** is to investigate the properties of the steady state resonance fluorescence emitted by a two-level atom embedded in a photonic bandgap crystal and driven by a classical pumping light. We treat the photon states in the photonic crystal as the background reservoir and obtain a set of generalized Bloch equations for the atomic operators by eliminating the reservoir field operators. The non-

uniform DOS distributions near the bandedge are modeled by the three-dimensional anisotropic dispersion relation [28] and the Liouville operator expansion is used to reduce the two-time atomic operator products into equal-time atomic operator products. In this way the nonlinear generalized Bloch equations are reduced into a set of linear equations with memory function terms caused by the atom-reservoir interaction. This set of linear equations can then be easily solved in the frequency domain and the resonance fluorescence spectra can be directly obtained from the correlation functions of the atomic operators in the frequency domain without applying the quantum regression theorem. After performing numerical calculation, we find that the spectral shape of the fluorescence intensity spectra will vary with the wavelength offset between the atomic transition wavelength and the bandedge. More interestingly, squeezing phenomena are found to be present in the in-phase quadrature spectra instead of the out-of-phase quadrature spectra.

2.2. Fluorescence Spectra

To begin the derivation, the Hamiltonian for the system to be considered can be written as:

$$H = \frac{\hbar\omega_a}{2}\sigma_z + \hbar\sum_k \omega_k a_k^\dagger a_k + \frac{\Omega\hbar}{2}(\sigma_- e^{i\omega_L t} + \sigma_+ e^{-i\omega_L t}) + \hbar\sum_k (g_k\sigma_+ a_k + g_k^* a_k^\dagger \sigma_-). \quad (2.1)$$

Here the transition frequency of the atom and the frequency of the pumping light are denoted by ω_a and ω_L respectively, $a_k^\dagger$ and a_k are the creation and annihilation

operators of the photon states in the photonic bandgap crystals, Ω is the Rabi-flopping frequency of the atom under the external pumping light and it also represents the relative magnitude of the pumping light, $\sigma_z \equiv (|2\rangle\langle 2| - |1\rangle\langle 1|)$, $\sigma_+ \equiv |2\rangle\langle 1| = \sigma_-^\dagger$ are the usual Pauli matrices for the two-level atom, and g_k is the atom-field coupling constant.

Starting from the Hamiltonian, we treat the photon field operators as the background reservoir and eliminate their corresponding equations to obtain the following set of generalized Bloch equations.

$$\dot{\sigma}_-(t) = i\frac{\Omega}{2}\sigma_z(t)e^{-i\Delta t} + \int_{-\infty}^{t} dt' G(t-t')\sigma_z(t)\sigma_-(t') + n_-(t), \quad (2.2)$$

$$\dot{\sigma}_+(t) = -i\frac{\Omega}{2}\sigma_z(t)e^{i\Delta t} + \int_{-\infty}^{t} dt' G_c(t-t')\sigma_+(t')\sigma_z(t) + n_+(t), \quad (2.3)$$

$$\dot{\sigma}_z(t) = i\Omega\left[\sigma_-(t)e^{i\Delta t} - \sigma_+(t)e^{-i\Delta t}\right] + n_z(t) \quad (2.4)$$

$$- 2\int_{-\infty}^{t} dt'[G(t-t')\sigma_+(t)\sigma_-(t') + G_c(t-t')\sigma_+(t')\sigma_-(t)].$$

Here $\Delta \equiv \omega_L - \omega_a$ and $\Delta_k \equiv \omega_a - \omega_k$. The two functions $G(\tau)$ and $G_c(\tau)$ are the memory functions of the system caused by the atom-reservoir interaction and they are defined as $G(\tau) \equiv \sum_k |g_k|^2 e^{i\Delta_k \tau}\Theta(\tau)$, and $G_c(\tau) \equiv \sum_k |g_k|^2 e^{-i\Delta_k \tau}\Theta(\tau)$. Here $n_-(t)$, $n_+(t)$, and $n_z(t)$ are three noise operators originated from the original photon filed operator before interaction.

Supposing that the reservoir is in thermal equilibrium, it can be easily shown that the three noise operators $n_-(t)$, $n_+(t)$, and $n_z(t)$ are zero mean with their correlation

functions given below:

$$\langle n_-(t)\rangle_R = \langle n_+(t)\rangle_R = \langle n_z(t)\rangle_R = \langle n_-(t)n_-(t')\rangle_R = \langle n_+(t)n_+(t')\rangle_R = 0, \quad (2.5)$$

$$\langle n_-(t)n_+(t')\rangle_R = \sum_k |g_k|^2 (\bar{n}_k + 1)e^{i\Delta_k(t-t')}\langle\sigma_z(t)\sigma_z(t')\rangle, \quad (2.6)$$

$$\langle n_+(t)n_-(t')\rangle_R = \sum_k |g_k|^2 \bar{n}_k e^{-i\Delta_k(t-t')}\langle\sigma_z(t)\sigma_z(t')\rangle, \quad (2.7)$$

$$\langle n_z(t)n_z(t')\rangle_R = 4\sum_k |g_k|^2 [(\bar{n}_k + 1)e^{i\Delta_k(t-t')}\langle\sigma_+(t)\sigma_-(t')\rangle \quad (2.8)$$
$$+ \bar{n}_k e^{-i\Delta_k(t-t')}\langle\sigma_-(t)\sigma_+(t')\rangle].$$

Since in general the correlation functions of these noise operators are not delta correlated at time (non-Markovian), we cannot directly use the Born-Markovian approximation to solve the problem. One can see that the correlation functions depend not only on the photon density of states, but also on the correlations of the atomic operators.

To actually evaluate the memory functions as well as the correlation functions of the noise operators, one needs to know the spectral distribution of the photonic density of states. Although in general the DOS of photonic bandgap crystals is very complicated and also varies with the geometrical structure and the dielectric constants of the material, it is still possible to approximately model the DOS near the bandedge with a simple formula. According to the results from the full vectorial numerical calculation, the DOS near the bandgap for three-dimensional photonic crystals increases from zero and behaves more like the anisotropic model proposed in the literature [28]. To be more specific, for a three dimensional photonic bandgap crystal, if the
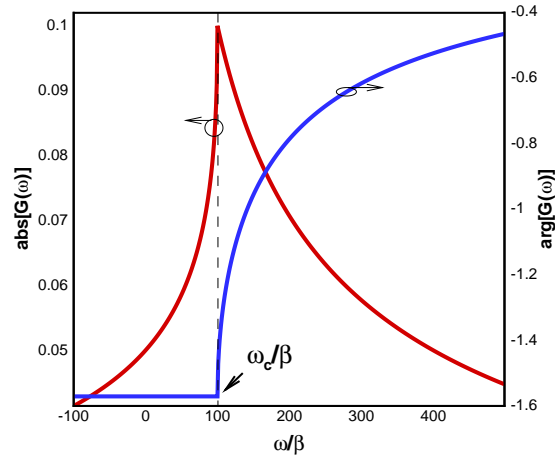
FIGURE 2.1: Amplitude and phase spectra of the memory function $G(\omega)$ with band-edge frequency $\omega_c = 100\beta$. The memory function is non-uniform around the bandedge and becomes pure imaginary inside the bandgap.

wavevector that corresponds to the bandedge is $\mathbf{k}_0^i$, then the dispersion relation in the anisotropic model is described by the following form: $\omega_k = \omega_c + A|\mathbf{k} - \mathbf{k}_0^i|^2$, where A is a model dependent constant and ω_c is the bandedge frequency. Based on this dispersion relation, the corresponding DOS is given by: $D(\omega) = \dfrac{1}{A^{3/2}}\sqrt{\omega - \omega_c}\,\Theta(\omega - \omega_c)$. The memory functions under this anisotropic model also can be derived as:

$$\tilde{G}(\omega) = \beta^{3/2}\frac{-i}{\sqrt{\omega_c} + \sqrt{\omega_c - \omega_a - \omega}}, \tag{2.9}$$

$$\tilde{G}_c(\omega) = \beta^{3/2}\frac{i}{\sqrt{\omega_c} + \sqrt{\omega_c - \omega_a + \omega}}. \tag{2.10}$$

where $\beta^{3/2} = \dfrac{\omega_a^2 d^2}{6\hbar\epsilon_0\pi A^{3/2}}\eta$, and we have used the space average coupling strength $\eta \equiv \dfrac{3}{8\pi}\displaystyle\int d\Omega |\hat{\mathbf{d}} \cdot \mathbf{E}|^2$ in the derivation.

From Fig. 2.1 the spectrum of the memory function $G(\omega)$ is non-uniform and asymmetric as we expect. When the frequency is far from the bandedge frequency ω_c,

the memory function is a pure real function which corresponding to the decay rate of

the atom. When the frequency is below the bandedge frequency, the memory function

becomes pure imaginary, indicating the inhibition of the spontaneous emission inside

the bandgap. And in between the memory function is a complex function, of which

the real part is related to the decay process and the imaginary part is related to the

oscillation process. The spectrum for another memory function $G_c(\omega)$ is also similar.

The generalized Bloch equations are a set of nonlinear operator equations and can-

not be solved easily. To overcome this difficulty, we introduce the following Liouville

operator expansion:

$$\sigma_{ij}(t) = e^{-iL(t-t')}\sigma_{ij}(t') = \sum_{n=0}^{\infty} \frac{[-i(t-t')]^n}{n!} L^n \sigma_{ij}(t'). \qquad (2.11)$$

Here the Liouville super operator L is defined as $L^n \sigma_{ij}(t') = \frac{1}{\hbar^n}[\cdots[\sigma_{ij}(t'), H], H], \cdots, H]$.

If the atom we consider is with a longer lifetime and under weak pumping (small Rabi

frequency), which is the usual case in the optical domain, then the time scale of the

atomic evolution will be longer than the time scale of the memory functions. There-

fore under such assumptions it should be legitimate to simply apply the zero-th order

perturbation term (zeroth-order Born approximation) [9]. This is equivalent to use

the equal time operator products to replace the two-time operator products. With

these approximations and by using the identities of Pauli matrices, the generalized

optical Bloch equations can be reduced into the following form:

$$\dot{\sigma}_-(t) = i\frac{\Omega}{2}\sigma_z(t)e^{-i\Delta t} - \int_{-\infty}^t dt' G(t-t')\sigma_-(t') + n_-(t), \qquad (2.12)$$

$$\dot{\sigma}_+(t) = -i\frac{\Omega}{2}\sigma_z(t)e^{i\Delta t} - \int_{-\infty}^t dt' G_c(t-t')\sigma_+(t') + n_+(t), \qquad (2.13)$$

$$\dot{\sigma}_z(t) = i\Omega(\sigma_-(t)e^{i\Delta t} - \sigma_+(t)e^{-i\Delta t}) \qquad (2.14)$$

$$- \int_{-\infty}^t dt'[G(t-t') + G_c(t-t')](1 + \sigma_z(t')) + n_z(t).$$

The approximation we have used should be valid as long as the time scale of the memory function is still much shorter than the time scale of the atomic response (i.e., the inverse of the Rabi frequency and the decay rate). It can be easily checked that the full-width-half-maximum (FWHM) bandwidth of the memory functions in Eq. (2.9) and Eq. (2.10) are $4\omega_c$. For a bandgap in the optical domain, the order of ω_c is about 10^{14-15} Hz, and the typical lifetime of the atom is from 10^{-3} sec to 10^{-9} sec, which is much longer than the response time of the memory functions.

Theoretically the fluorescence spectrum can be calculated by taking the Fourier transform of the first order correlation function of the atomic dipole moment operator. By using Fourier transform, we can directly solve these modified optical Bloch equations in Eq. (2.12). Because the two-time correlation function of the atomic dipole is proportional to the first order coherence function $g^{(1)}(\tau)$ [29] of the radiated photon field and the fluorescence spectrum can be obtained by taking the Fourier transform of the first order coherence function, one has:

$$S(\omega) = \int_{-\infty}^\infty d\tau\, g^{(1)}(\tau)e^{i\omega\tau} \propto \langle\tilde{\sigma}_+(\omega)\tilde{\sigma}_-(-\omega)\rangle_R. \qquad (2.15)$$
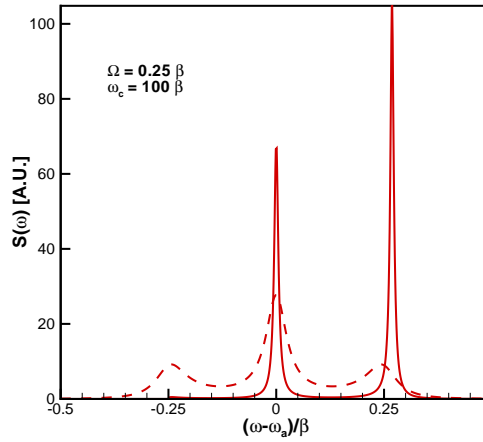
FIGURE 2.2: Comparison of resonance fluorescence spectra far from the bandedge (dashed-line, $\omega_a - \omega_c = 1000\beta$) and near the bandedge (solid-line $\omega_a - \omega_c = \Omega$); $\Omega = 0.25\beta$, $\omega_c = 100\beta$.

In this way the fluorescence spectrum can be easily determined after determining the noise correlation functions. By using the anisotropic model from Eqs. (2.9, 2.10), it can be easily to show that the statistics of the quantum noises of the photonic bandgap reservoir are not only color noises but also exhibit bandgap behavior.

Based on the above formula, in Fig. 2.2 we plot the resonance fluorescence spectra at a constant Rabi frequency when the atomic transition frequencies ω_a are far from (dashed-line) and near (solid-line) the bandedge frequency ω_c respectively. The evolution of the resonance fluorescence spectra with different offsets between the transition frequency and the bandedge frequency are also plotted in Fig. 2.3. It can be noted that the separation of each adjacent peaks is determined by the Rabi frequency as in the case of free space. When the atomic transition frequency is far away from the
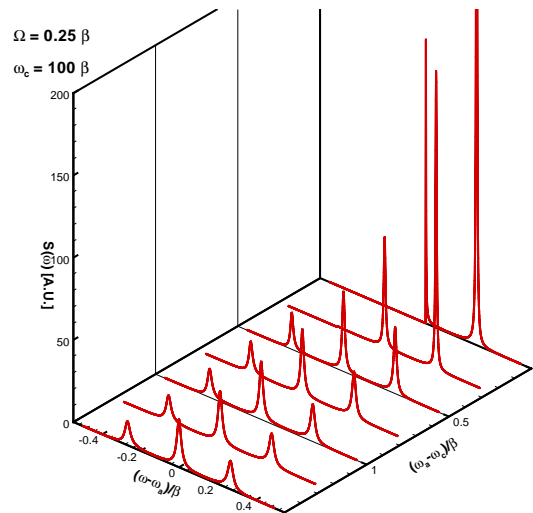
FIGURE 2.3: Evolution of resonance fluorescence spectrum near the bandedge at constant Rabi frequency: $\Omega = 0.25\beta$, $\omega_c = 100\beta$.

bandedge ($\omega_a \gg \omega_c$), the normal resonance fluorescence spectrum of Mollow's triplets with three Lorentzian profiles is obtained just as expected [18]. The contribution from the elastic Rayleigh scattering in the center part (which is a delta function with zero detuning frequency) has been ignored and only the contribution from the inelastic Raman scattering (the three peaked profiles) are considered here. The linewidth of each peak is proportional to the decay rate of atom and the separation of adjacent peaks is proportional to the Rabi frequency.

When the atomic transition frequency moving toward the bandedge, the profiles due to incoherent scattering processes become sharper and sharper because there are fewer and fewer DOS available. The narrowing of the fluorescence spectra also indicates a smaller decay rate due to the forbidden effect of the bandgap. The profile in the lower frequency is not only suppressed but also becomes asymmetrical due to

the existence of the bandgap. It should also be noted that the peak in the higher frequency is enhanced a lot as can be clearly seen in the figure. Eventually the peak in the lower frequency will be totally suppressed when the atomic transition frequency is moving more toward the bandedge. At this time the resonance fluorescence spectrum now only has two peaks.

2.3. Fluorescence Squeezing Spectra

The noise spectra of a two-level atom driven by a classical pumping light can also exhibit non-classical phenomena (squeezing spectra) if the phase-dependent fluorescence spectra are measured. To observe squeezing in the phase-dependent fluorescence spectra, one needs to calculate the fluorescence spectra for the quadrature field components. Theoretically the quadrature field operator in the θ phase angle is defined as, $\hat{E}_\theta(t) = e^{i\theta}\hat{E}^{(+)}(t) + e^{-i\theta}\hat{E}^{(-)}(t)$. The two cases corresponding to $\theta = 0$ and $\theta = \pi/2$ represent the in-phase and out-of-phase components of the electric field respectively. The spectra for the quadrature fields can be obtained by calculating the following normally order variance:

$$
\begin{aligned}
S_\theta(\omega) &\equiv\ < \tilde{E}_\theta(\omega), \tilde{E}_\theta(-\omega) >, &(2.16)\\
&=\ \Gamma\frac{1}{4}[< \tilde{\sigma}_-(\omega)\tilde{\sigma}_-(-\omega) > e^{-2i\theta} + < \tilde{\sigma}_+(\omega)\tilde{\sigma}_-(-\omega) >\\
&+\ < \tilde{\sigma}_+(-\omega)\tilde{\sigma}_-(\omega) > + < \tilde{\sigma}_+(-\omega)\tilde{\sigma}_+(\omega) > e^{2i\theta}].
\end{aligned}
$$

where the correlation functions have been renormalized with the total outgoing flux
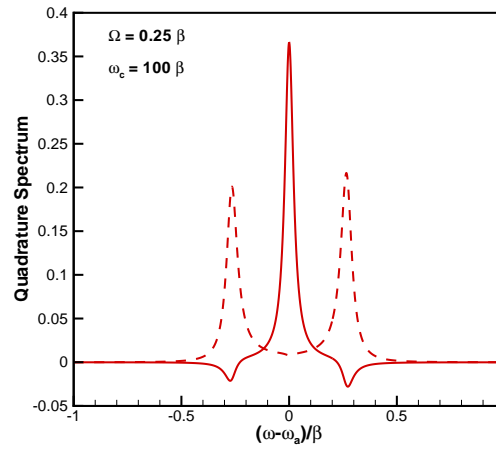
FIGURE 2.4: Resonance fluorescence quadrature spectra near the bandedge; Solid line: in-phase, $S_1(\omega)$, Dashed line: out-of-phase, $S_2(\omega)$ with $\omega_c = 100\beta$ and $\Omega = 0.25\beta$.

and Γ is the decay rate of the two-level atom [24, 25].

In the free space case, the in-phase quadrature $S_1(\omega)$ produces the central peak of the Mollow's triplet while the out-of-phase quadrature $S_2(\omega)$ produces the two side-peaks when the separation of the two sidebands is large. When the Rabi frequency is small (small driving field), $\Omega^2 < 4\Gamma^2$, squeezing can be observed in the out-of-phase quadrature spectra.

The situations are different for the case of photonic bandgap crystals. When the transition frequency is near the bandedge of the photonic crystals, the bandgap effects modify the fluorescence intensity spectrum and cause asymmetric spectral profiles as we have seen in Fig. (2.2). As shown in Fig. 2.4, for the case of photonic bandgap crystals, the in-phase quadrature not only contributes to the central component but
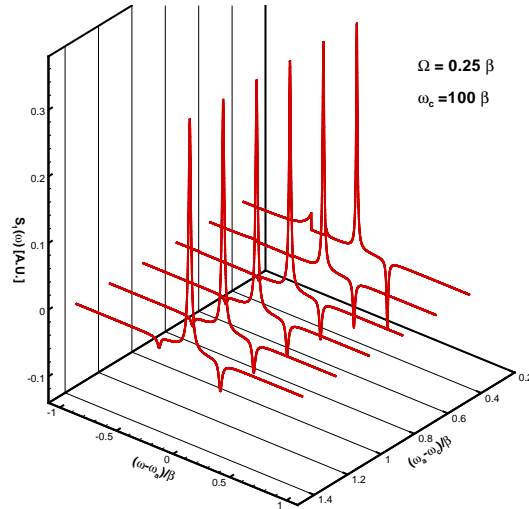
FIGURE 2.5: Evolution of in-phase quadrature spectra near the bandedge with $\omega_c = 100\beta$ and $\Omega = 0.25\beta$.

also the two sidebands. The out-of-phase quadrature still only contributes to the two sidebands as in the case of free space. Moreover, we find both sidebands of the in-phase quadrature now exhibit squeezing even when $\Omega^2 > 4\Gamma^2$. This squeezing effect in the in-phase quadrature near the bandedge is similar to the case of a atom dressed by the finite-bandwidth cavity-field excitation [30].

In the above calculation all the quadrature noise spectra are normalized with respect to the decay rate of the atom, Γ, as shown in Eq. (2.16). For the case of free space, the decay rate Γ is frequency independent due to the white noise reservoir. However, for photonic crystals, the decay rate will be modified according to the offset between the atomic transition frequency and the bandedge frequency. According to the works in references [5, 9], the spontaneous emission rate of a two-level atom near the bandedge contains non-exponential terms. For simplicity we have used the

following formula to estimate the decay rate of the atom:

$$\Gamma \quad \approx \quad \text{Re}[\tilde{G}(\omega = 0)] = \beta^{3/2}\frac{\sqrt{\omega_a - \omega_c}}{\omega_a} \tag{2.17}$$

In Fig. (2.5), we plot the evolution of the in-phase quadrature spectra for different frequency (wavelength) offset. One can see that the higher frequency peak exhibits larger squeezing as well as larger fluorescence intensity when the offset frequency is approaching the bandedge frequency.

<u>2.4. Summary</u>

In summary, by introducing the Liouville operator expansion, we have successfully overcome some of the difficulties associated with the non-Markovian nature of the problem caused by the non-uniform distribution of the photon states in the photonic bandgap crystal. Our calculated results have indicated that the resonance fluorescence spectra near a photonic bandgap can exhibit interesting behavior including the suppression and enhancement of the Mollow's triplet peaks, and the squeezing phenomena in the in-phase quadrature spectra. Besides the atom-light interaction in the *linear* photonic crystals, in next **Chapter** we will switch the gear to discuss quantum properties of waves in *nonlinear* PhCs, which can support unique wave solutions - the gap solitons.

CHAPTER 3

Quantum theory of Bragg solitons and gap solitons

3.1. Introduction

In the literature, various types of optical soliton phenomena have been studied extensively in the area of nonlinear optical physics. These include the nonlinear Schrödinger solitons in dispersive optical fibers, spatial and vortex solitons in photorefractive materials/waveguides, and cavity solitons in resonators [31]. Gap solitons are also found to exist in nonlinear periodic systems due to combination of unique properties of nonlinear periodic systems.

In fiber optics, it has been well known that fiber Bragg gratings (FBGs) with Kerr nonlinearity can exhibit optical soliton-like phenomena known as the fiber Bragg grating solitons [10, 32]. The FBGs are one-dimensional photonic bandgap crystals with weak index modulation. By utilizing the high dispersion of the FBGs near the bandedges, one can produce optical solitons in the anomalous dispersion spectral side if the input pulse have suitable pulse-width and peak intensity.

From the theoretical point of view, fiber Bragg grating solitons belong to the class of bi-directional pulse propagation problems, where the quantum theory is still lack of enough consideration. Most of the previous studies on fiber Bragg grating

solitons have been on the classical effects and there is almost no reported result on their quantum properties. The quantum theory of traveling-wave optical solitons has been intensively developed during the past 15 years and several approaches have been successfully carried out to calculate the quantum properties of different traveling-wave optical solitons including the family of nonlinear Schrödinger solitons [33, 34, 35, 36, 37] as well as the self-induced-transparency solitons [38]. In the first part of this **Chapter**, we develop a general quantum theory for bi-directional pulse propagation problems and particularly by applying the theory to the case of fiber Bragg grating solitons. It will be shown that the fiber Bragg grating soliton pulses will quantum-mechanically get amplitude-squeezed after passing through the fiber grating and the squeezing ratio will be calculated theoretically. The squeezing ratio of FBG solitons is found to exhibit interesting relations with the fiber grating length as well as with the intensity of the input pulse. With the use of apodized FBGs, we also find that one can tailor the squeezing ratio of FBG solitons al long as the soliton pulses evolve adiabatically.

More generally, FBG solitary waves are only a subset of gap solitons in shallow periodic media. For examples, supported by the nonlinear photonic bandgap crystals made of Kerr materials [11, 12], or by loading Bose-Einstein condensates (BEC) into an optical lattices [13, 39, 40, 41], optical and matter-wave gap solitons have been predicted to display lots of novel nonlinear optical phenomena. Recently, demonstrations of optical gap solitons in the dynamically reconfigurable PhCs [42, 43, 44]

and bright gap solitons of an attractive or a repulsive BEC in an optical potential [15, 45, 46] show that the dynamics of these system are very rich and complex.

In the second part of this **Chapter**, we will study the quantum fluctuations of matter-wave gap solitons in an optical lattice and investigate the band-gap effects on quantum noise squeezing. We employ the soliton perturbation approach [16] to analyze quantum fluctuations around the soliton solutions of Gross-Pitaevskii equation (GPE) with a periodic potential. Using this approach, we demonstrate the enhancement of quantum noise squeezing induced by gap soliton evolution in an atomic band-gap structure.

3.2. Quantum theory of FBG solitons

In our modeling, we use the nonlinear coupled mode equations (NCMEs) to describe the bi-directional waves propagating in a uniform FBG. To be more explicit, let us consider the wave propagation problem in a one dimension fiber grating structure with the nonlinearity coming from the third order nonlinearity of the optical fiber. With the self-phase modulation and cross-phase modulation effects, we model Bragg solitons by using the following NCMEs that describe the coupling between the forward and the backward propagating waves in a uniform FBG.

$$\frac{1}{v_g}\frac{\partial}{\partial t}U_a(z,t) + \frac{\partial}{\partial z}U_a = i\delta U_a + i\kappa U_b + i\Gamma|U_a|^2 U_a + 2i\Gamma|U_b|^2 U_a, \tag{3.1}$$

$$\frac{1}{v_g}\frac{\partial}{\partial t}U_b(z,t) - \frac{\partial}{\partial z}U_b = i\delta U_b + i\kappa U_a + i\Gamma|U_b|^2 U_b + 2i\Gamma|U_a|^2 U_b. \tag{3.2}$$

Here $U_a(z,t)$ and $U_b(z,t)$ represent the forward and backward propagation pulses respectively. They are in the units of $GW^{1/2}/cm$. Moreover, v_g is the group velocity of the pulse, κ is the coupling coefficient, λ_B is the Bragg wavelength, δ is the wavelength detuning parameter, and Γ represents the self-phase modulation coefficient.

This set of NCMEs has analytical soliton solutions for the case of infinite grating length, as is shown by Aceves and Wabnitz with the introduction of the massive Thirring model [10]. However, for gratings of finite length, no analytic solution can be found. So in our studies we directly use the finite difference numerical simulation method with the parameters based on the first experimental reported in the literature [32]. We consider a 60 ps FWHM *sech*-shaped pulse incidents into a uniform grating with 15.0 cm^{-1} wavenumber detuning from the center of the bandgap. The coupling strength of the fiber grating is 10 cm^{-1}, the nonlinear coefficient Γ is 0.018 cm/GW, and the group velocity v_g is chosen to be c/n with $n = 1.5$ and c being the speed of light in free space. When the input peak intensity is below the required value for forming a solitary pulse in the FBGs (about 4.5 GW/cm^2 in this case), the peak intensity of the pulse will decrease along the propagation. On the other hand, as shown in Fig. 3.1, when the input peak intensity is above 4.5 GW/cm^2, the peak intensity of the pulse oscillates during the propagation within the grating. Only when the nonlinearity can exactly compensate the dispersion induced by the FBGs, one can have a stable solitary pulse inside the grating.

After obtaining these classical solutions, we now turn to the calculation of their
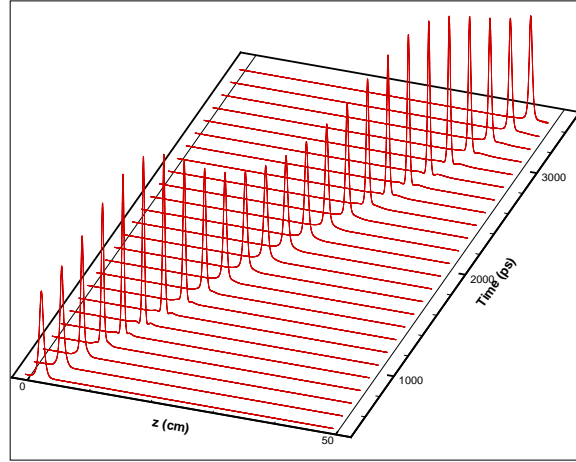
FIGURE 3.1: Evolution of the fiber Bragg grating soliton with the input peak intensity $I = 9.0 GW/cm^2$.

quantum properties. In quantum theory the NCMEs become the quantum nonlinear coupled mode equations (QNCMEs):

$$\frac{1}{v_g}\frac{\partial}{\partial t}\hat{U}_a(z,t) + \frac{\partial}{\partial z}\hat{U}_a = i\delta\hat{U}_a + i\kappa\hat{U}_b + i\Gamma\hat{U}_a^\dagger\hat{U}_a\hat{U}_a + 2i\Gamma\hat{U}_b^\dagger\hat{U}_b\hat{U}_a, \tag{3.3}$$

$$\frac{1}{v_g}\frac{\partial}{\partial t}\hat{U}_b(z,t) - \frac{\partial}{\partial z}\hat{U}_b = i\delta\hat{U}_b + i\kappa\hat{U}_a + i\Gamma\hat{U}_b^\dagger\hat{U}_b\hat{U}_b + 2i\Gamma\hat{U}_a^\dagger\hat{U}_a\hat{U}_b, \tag{3.4}$$

where $\hat{U}_a$ and $\hat{U}_b$ represent the forward and backward normalized fields which satisfy the usual equal time Bosonic commutation relations.

$$[\hat{U}_a(z_1,t), \hat{U}_a^\dagger(z_2,t)] = \delta(z_1 - z_2),$$

$$[\hat{U}_b(z_1,t), \hat{U}_b^\dagger(z_2,t)] = \delta(z_1 - z_2),$$

$$[\hat{U}_a(z_1,t), \hat{U}_a(z_2,t)] = [\hat{U}_a^\dagger(z_1,t), \hat{U}_a^\dagger(z_2,t)] = 0,$$

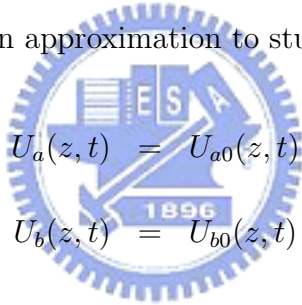$$[\hat{U}_b(z_1,t), \hat{U}_b(z_2,t)] = [\hat{U}_b^\dagger(z_1,t), \hat{U}_b^\dagger(z_2,t)] = 0,$$

$$[\hat{U}_a(z_1,t), \hat{U}_b(z_2,t)] = [\hat{U}_a(z_1,t), \hat{U}_b^\dagger(z_2,t)] = 0.$$

This is a set of coupled operator equations in the Heisenberg picture and can be derived from the following Hamiltonian under the effective-mass approximation [47]

$$
\begin{aligned}
H &= -v_g \{ \delta \int dz \, (\hat{U}_a^\dagger \hat{U}_a + \hat{U}_b^\dagger \hat{U}_b) + i \int dz \, (\hat{U}_a^\dagger \frac{\partial}{\partial z} \hat{U}_a - \hat{U}_b^\dagger \frac{\partial}{\partial z} \hat{U}_b) \\
&+ \kappa \int dz \, (\hat{U}_a^\dagger \hat{U}_b + \hat{U}_b^\dagger \hat{U}_a) + \frac{\Gamma}{2} \int dz \, (\hat{U}_a^\dagger \hat{U}_a^\dagger \hat{U}_a \hat{U}_a + \hat{U}_b^\dagger \hat{U}_b^\dagger \hat{U}_b \hat{U}_b) \\
&+ \Gamma \int dz \, (\hat{U}_a^\dagger \hat{U}_b^\dagger \hat{U}_b \hat{U}_a + \hat{U}_b^\dagger \hat{U}_a^\dagger \hat{U}_a \hat{U}_b) \}.
\end{aligned}
\tag{3.5}
$$

This derivation automatically proves that the QNCMEs preserve the commutation brackets.

Since for optical solitons the average photon number is usually very large, we can safely use the linearization approximation to study their quantum effects. By setting

$$
\begin{aligned}
U_a(z,t) &= U_{a0}(z,t) + \hat{u}_a(z,t), \\
U_b(z,t) &= U_{b0}(z,t) + \hat{u}_b(z,t),
\end{aligned}
$$

and substituting them into Eq. (3.3-3.4) for linearization, we obtain the linear quantum operator equations in Eq. (3.6) that describe the evolution of the quantum fluctuations associated with the fiber Bragg grating solitons. The quantum perturbation fields $\hat{u}_a(z,t)$ and $\hat{u}_b(z,t)$ in Eq. (3.6) also have to satisfy the same equal time

commutation relations as the original field operators $\hat{U}_a(z,t)$ and $\hat{U}_b(z,t)$.

$$\frac{1}{v_g}\frac{\partial}{\partial t}\begin{pmatrix} \hat{u}_a \\ \hat{u}_b \end{pmatrix} = \begin{pmatrix} i\Gamma U_{a0}^2 & 2i\Gamma U_{a0}U_{b0} \\ 2i\Gamma U_{a0}U_{b0} & i\Gamma U_{b0}^2 \end{pmatrix}\begin{pmatrix} \hat{u}_a^\dagger \\ \hat{u}_b^\dagger \end{pmatrix} + \tag{3.6}$$

$$\begin{pmatrix} -\dfrac{\partial}{\partial z} + i\delta + 2i\Gamma|U_{a0}|^2 + 2i\Gamma|U_{b0}|^2 & i\kappa + 2i\Gamma U_{a0}U_{b0}^* \\[2ex] i\kappa + 2i\Gamma U_{a0}^* U_{b0} & \dfrac{\partial}{\partial z} + i\delta + 2i\Gamma|U_{a0}|^2 + 2i\Gamma|U_{b0}|^2 \end{pmatrix}\begin{pmatrix} \hat{u}_a \\ \hat{u}_b \end{pmatrix},$$

$$\frac{1}{v_g}\frac{\partial}{\partial t}\begin{pmatrix} u_a^A \\ u_b^A \end{pmatrix} = \begin{pmatrix} -i\Gamma U_{a0}^2 & -2i\Gamma U_{a0}U_{b0} \\ -2i\Gamma U_{a0}U_{b0} & -i\Gamma U_{b0}^2 \end{pmatrix}\begin{pmatrix} u_a^{A*} \\ u_b^{A*} \end{pmatrix} + \tag{3.7}$$

$$\begin{pmatrix} -\dfrac{\partial}{\partial z} + i\delta + 2i\Gamma|U_{a0}|^2 + 2i\Gamma|U_{b0}|^2 & i\kappa + 2i\Gamma U_{a0}U_{b0}^* \\[2ex] i\kappa + 2i\Gamma U_{a0}^* U_{b0} & \dfrac{\partial}{\partial z} + i\delta + 2i\Gamma|U_{a0}|^2 + 2i\Gamma|U_{b0}|^2 \end{pmatrix}\begin{pmatrix} u_a^A \\ u_b^A \end{pmatrix}.$$

If we define the inner product operation according to

$$\langle \vec{f}|\vec{\hat{g}}\rangle = \frac{1}{2}\int dz\,[f_a^*\hat{g}_a + f_a\hat{g}_a^\dagger + f_b^*\hat{g}_b + f_b\hat{g}_b^\dagger], \tag{3.8}$$

then Eq. (3.7) is the corresponding set of adjoint equations for the perturbed QNCMEs, which have the following desired property:

$$\frac{d}{dt}\langle \vec{u}^A|\vec{\hat{u}}\rangle = 0, \tag{3.9}$$

where $\vec{u}^A = (u_a^A, u_b^A)^T$ is the solution of the adjoint equation defined in Eq. (3.7). The important thing is that the inner product between the solutions of the two equation sets is preserved along the time axis.

By taking advantage of the preservation of the inner product, we can express the inner product of the output quantum perturbation operator with a projection function in terms of the input quantum field operators by the *back-propagation method*.
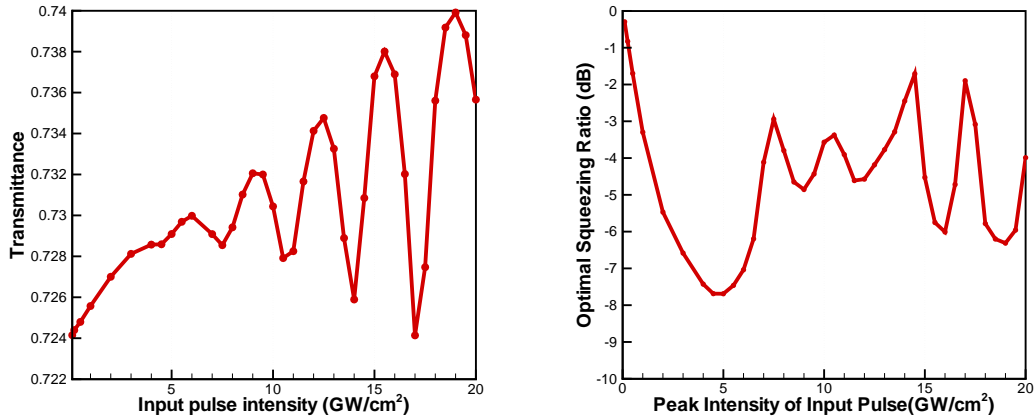
FIGURE 3.2: Transmittance (left) and photon number squeezing ratio (right) for fiber Bragg grating solitons with different input intensities.

This will allow us to calculate the quantum uncertainty for the inner product of the output quantum operator with any given projection function. Under the linearization approximation, any measurement of a physical quantity can be expressed as an inner product between a measurement characteristic function and the perturbed quantum field operator [16]. The squeezing ratio of the measured quantity thus can be calculated according to:

$$R(T) = \frac{var[\langle \vec{f}|\vec{\hat{u}}(t=T)\rangle]}{var[\langle \vec{f}|\vec{\hat{u}}(t=0)\rangle]} = \frac{var[\langle \vec{F}_T|\vec{\hat{u}}(t=0)\rangle]}{var[\langle \vec{f}|\vec{\hat{u}}(t=0)\rangle]}. \tag{3.10}$$

Here $var[\cdot]$ means the variance, $\vec{f}$ is the original projection function and $\vec{F}_T$ is the back-propagated projection function. The choice of the characteristic function $\vec{f}$ will depend on the measurement to be performed. For the photon number measurement, $\vec{f}$ is simply the normalized output classical pulse from the grating [48]. For the homodyne detection, it will be the local oscillator pulse. In the following we consider
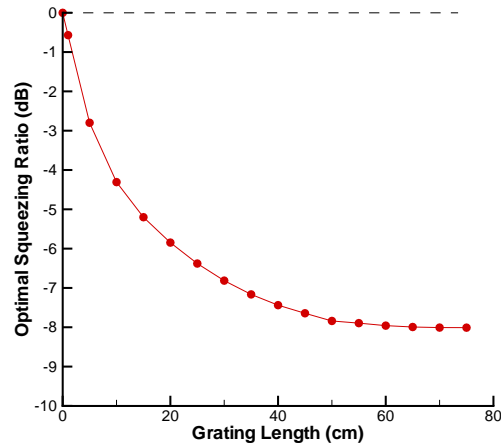
FIGURE 3.3: Optimal squeezing ratio for Bragg solitons propagating through different length of FBGs.

a solitary pulse incident into a uniform FBG, and calculate the quantum fluctuation of its first transmitted pulse based on the formulation given above.

The transmittance of the FBGs with different input intensities of solitons for a constant FBG length (50 cm) is shown in the top curve of Fig. 3.2. The calculated photon number squeezing ratio is shown in the bottom for the same parameters. When the input peak intensity is smaller than that of the fundamental soliton, the output squeezing ratio monotonically decreases when the input peak intensity is increased. The output squeezing ratio will begin to oscillate strongly with respect to the changing input intensity when the input intensity is much larger than that of the fundamental soliton. The oscillation behaviors of the FBG transmittance and the squeezing ratio match very well. That is, the squeezing ratio has a local minimum when the transmission has a local maximum. Intuitively the periodic grating structure
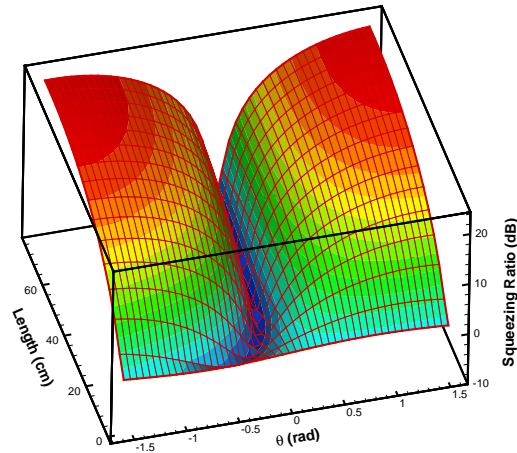
FIGURE 3.4: Squeezing ratio for different FBG lengths and different local oscillator phases.

acts like a spectral filter which can filter out the noisier high frequency components in the soliton spectrum and produce a net amplitude squeezing effect just as in the previous soliton amplitude squeezing experiments where a spectral filter is cascaded after a nonlinear fiber [49, 50]. And the minimum squeezing ratio occurs when the pulse energy of soliton is slightly large than that of the fundamental soliton. It is also intuitively clear that larger amplitude squeezing should occur when the transmittance curve is saturated. Fig. 3.3 shows the dependence of the optimal squeezing ratios for different FBG lengths with a constant input intensity ($I = 4.5GW/cm^2$). If we only consider the gratings with the length longer than 1 cm, we find that the squeezing ratio monotonically decreases with the FBG length and saturates at the length around 60 cm. Intuitively this is because the filtering effect of the grating will unavoidably introduce additional noises on the light fields and eventually cause the

squeezing ratio to become saturated.

So far we have shown that the FBG solitons will get amplitude squeezed during propagation. Under the linearization approximation, the amplitude squeezing corresponds to the squeezing of the in-phase quadrature field component. To further determine the maximum squeezing phase angle of the quadrature field components of the FBG solitons, we perform another calculation to simulate the squeezing ratio when the homodyne detection scheme is used and when the local oscillator pulse is exactly the classical output pulses. With the homodyne detection scheme, one has the additional degree of freedom to adjust the relative phase between the local oscillator and the signal for detecting different quadrature field components. Fig. 3.4 plots the squeezing ratio for different FBG lengths and for different local oscillator phases with a constant input intensity ($I = 4.5 GW/cm^2$). One can see that for short FBG lengths the quadrature squeezing direction is close to but not exactly in the in-phase (or amplitude) quadrature, $\theta = 0$. However, when the FBG length is long enough, the squeezing direction will approach the in-phase quadrature. This proves that the FBG solitons will indeed be squeezed in the amplitude direction when the FBG length is long enough.

In Fig. 3.5 we illustrate the possible direct detection scheme for measuring the photon number squeezing of the FBG solitons. To avoid the complication due to the multiple transmitted pulses of the FBG, it may be necessary to use a time-gating device to make sure that only the first transmitted pulse is detected
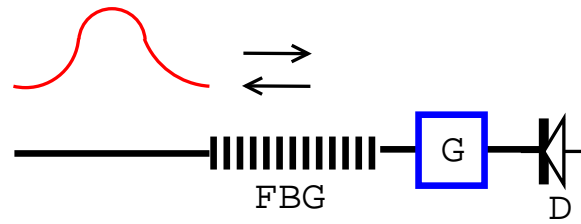
FIGURE 3.5: Measurement scheme of direct detection for observing FBG soliton squeezing. Here G is a gating device which will block out all the transmitting pulses but the first one; D is an optical detector.

It is well known that one can engineer the dispersion along the FBG by using an *apodized* FBG. Such apodized nonlinear FBGs have been used for adiabatic soliton pulse compression within a very short length of several centimeters [51]. Intuitively the solitons with higher peak intensities will exhibit large squeezing due to higher nonlinear effects. It is thus expected to be able to compress the pulsewidth of the FBG soliton and enhance its squeezing ratio simultaneously. To verify this idea, here we consider an apodized FBG which has a position dependent coupling coefficient described by

$$\kappa(z) = \kappa_0 + \alpha z, \tag{3.11}$$

where $\kappa_0 = \omega_0 \tilde{\epsilon}/2\bar{n}c$ is the initial coupling coefficient and α is the slope of the coupling coefficient.

In the following calculation we consider the same 60 *ps* FWHM *sech*-shaped input pulse with the peak intensity of $I = 4.5 GW/cm^2$ for the apodized grating without changing any parameter. In Fig. 3.6 (Left) we plot the squeezing ratio versus the FBG length with a constant input intensity ($I = 4.5 GW/cm^2$) and different apodization
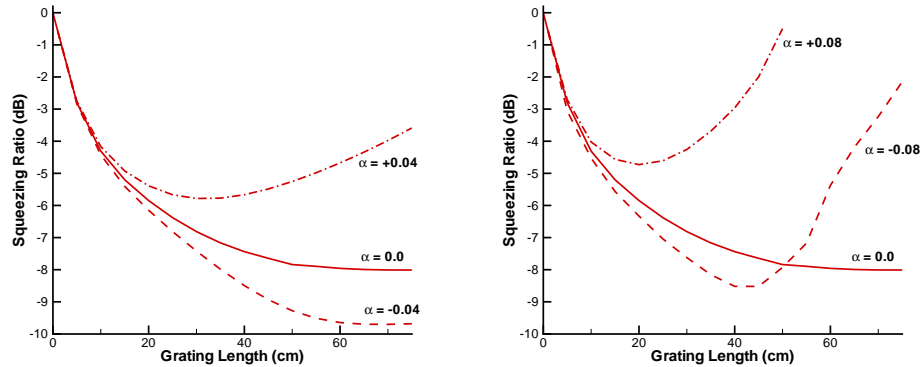
FIGURE 3.6: Photon number squeezing ratio versus the FBG length with a constant input intensity ($I = 4.5GW/cm^2$). (Left): The three curves correspond to different slopes of $\kappa(z)$; Solid-line: $\alpha = 0$; Dashed-line: $\alpha = -0.04$; Dash-dotted line: $\alpha = +0.04$. (Right): Solid-line: $\alpha = 0$; Dashed-line: $\alpha = -0.08$; Dash-dotted line: $\alpha = +0.08$.

slopes. The three curves in Fig. 3.6 (Left) correspond to different slops of $\kappa(z)$: $\alpha = +0.04, 0, -0.04$ respectively. When $\alpha = 0.04(1/cm^{-2})$, the FWHM of the original FBG soliton (60 ps) will be adiabatically compressed into 30 ps after propagating through a 70 cm FBG. Because of this, the achievable optimal squeezing ratio thus increases from 8 dB to 9.7 dB for the propagation distance of 70 cm. On the other hand, if the slope of the coupling coefficient is positive, we have a broaden FBG soliton and the optimal squeezing ratio will be degraded. If the slope of the coupling coefficient is too large, then the soliton cannot be compressed adiabatically and thus the optimal squeezing ratio will be degraded eventually. This can be seen in Fig. 3.6 (Right), where we plot the squeezing ratio versus the grating length with larger slopes ($\alpha = -0.08, +0.08$). The result for the uniform FBG case ($\alpha = 0$) is also plotted for

comparison.

3.3. Quantum theory of gap solitons

Due to similarities between the physics of atomic solitons in *attractive* BEC and optical solitons in a Kerr medium, the two systems are expected to have similar quantum noise properties. It has been recognized [52] that general methods of quantum noise squeezing and entanglement developed in quantum optics could apply to other nonlinear bosonic fields, such as weakly interacting ultracold atoms in a Bose-Einstein condensate (BEC). Consequently, a number of theoretical proposals were put forward [53, 54] and some experiments were carried out [55, 56, 57] for generating macroscopic entangled number-squeezed states in BEC. Production of the quantum correlations among the macroscopic quantum states relies on the nonlinear interaction of the atomic waves. The mechanism is analogous to the production of squeezing through optical Kerr nonlinearity.

For instance, particle number squeezing of an atomic soliton during its evolution may result from coupling between the soliton amplitude and phase, akin to those induced in optical solitons formed through the Kerr nonlinearity [58, 59]. Recently, however, a new kind of *gap solitons* in a *repulsive* condensate, supported in periodic potentials of optical lattices, have attracted a great deal of attention due to their potential for controllable interaction and robust evolution uninhibited by collapse [13, 15, 39, 40, 41]. The current techniques for gap solitons generation suffer greatly
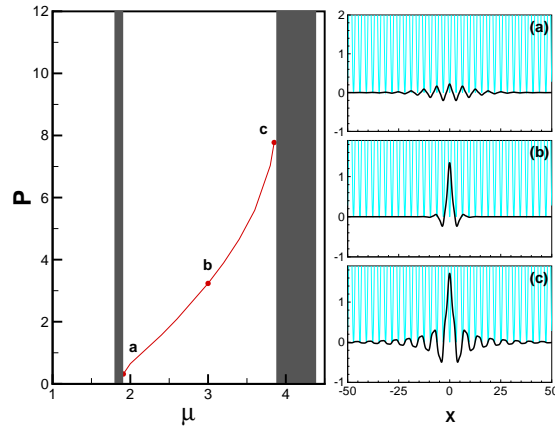
FIGURE 3.7: Left: Band-gap diagram for Bloch waves (bands are shaded), and the family of the gap solitons in the first finite gap for $V_0 = 4.0$. Right: Profiles of gap solitons with different chemical potentials; $\mu = 1.91$, 3.0, and 3.85 corresponding to the points a, b, and c respectively.

from "technical" noise [15]. Provided this problem can eventually be overcome, e.g. by employing low-noise stabilized atom laser sources [60], gap solitons may represent an attractive high-density source for atomic interferometry, quantum measurements and quantum information processing with ultracold atoms. To understand and control the quantum noise associated with atomic gap solitons are therefore fundamental issues which so far have not been explored.

As a model, we consider an elongated cigar-shape BEC loaded into a one-dimensional optical lattice and described by the mean-field Gross-Pitaevskii equation for the macroscopic wave function (see, e.g. Ref. [40]):

$$i\hbar\frac{\partial\Psi}{\partial t} = -\frac{1}{2}\frac{\partial^2\Psi}{\partial x^2} + V(x)\Psi + g_{1D}|\Psi|^2\Psi, \qquad (3.12)$$

where Ψ is the normalized macroscopic wave function of the condensate, g_{1D} is the

nonlinear interaction coefficient, and $V(x) = V_0 \sin^2(x)$ is the one-dimensional periodic potential. Stationary states of the condensate can be presented in the form, $\Psi(t,x) = \psi(x)\exp(-i\mu t)$, where μ is the chemical potential. In the linear, non-interacting limit, $g_{1D} \to 0$, the spectrum of matter waves has the characteristic band-gap structure [40]. The nonlinear localization of matter waves in the form of *gap solitons* occurs in the gaps of the linear spectrum, and the family of the lowest-order gap solitons in the first (finite) spectral gap is shown in Fig. 3.7 as the dependence of the soliton norm, $P = \int \psi^2 dx$, vs. chemical potential.

It is well known that the degree of localization of gap solitons varies across the gap [see Fig. 3.7(a-c)]. Near the bottom edge of the gap, $\mu \approx \mu_0$ the weakly localized soliton profile is well described by the "envelope" approximation [61],

$$\psi(x;\mu) = AF(x)\Phi(x;\mu_0), \tag{3.13}$$

where $\Phi(x;\mu_0)$ is the periodic Bloch state at the corresponding band edge and $F(x)$ is a slowly varying function of the spatial coordinate. The inset of Fig. 3.8 shows the oscillating wavefunction $\psi(x)$ of a gap soliton near the band edge, at $\mu = 1.91$, together with the corresponding Bloch-wave envelope $F(x)$. The envelope function $F(x)$ is the solution of the lattice-free GPE or nonlinear Schrödinger (NLS) equation with the effective *anomalous* diffraction and interaction energy modified by the lattice [61].

To study the quantum fluctuations of the gap solitons, we replace the 'classical' mean field described by Eq. (3.12) by the bosonic field operator $\hat{\Psi}$. Then, we use
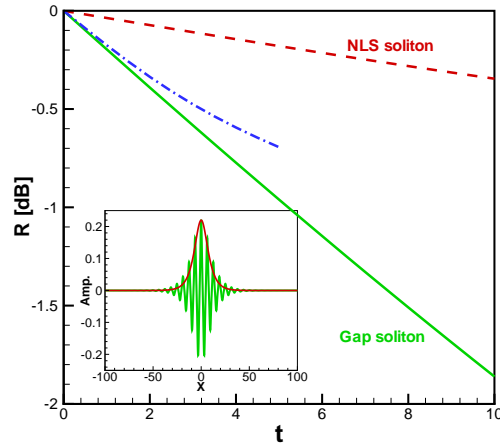
FIGURE 3.8: Time evolution of the optimal squeezing ratio, R, for the gap soliton (solid), its near-band-edge envelope approximation (dot-dashed), and the envelope (NLS) soliton (dashed). Inset: profiles of the gap soliton found from Eq. (3.12) at $\mu = 1.91$ and its envelope used in approximation of Eq. (3.13).

the linearization approach with the perturbed quantum field operator $\hat{\psi}$ around the mean-field solution Ψ_0. By using the *back-propagation method* [16], we calculate the optimal squeezing ratio for gap solitons as a function of the evolution time. The optimal squeezing ratio of the quadrature field for gap solitons, as a result of the homodyne detection scheme, can be defined as the ratio of variances [16]:

$$R(t) = \min[\text{var}\langle \Psi_L(t)|\hat{\psi}(t)\rangle / \text{var}\langle \Psi_L(t)|\hat{\psi}(0)\rangle],$$

where the inner product between the operator perturbation field, $\hat{\psi}$, and the local oscillator profile, Ψ_L, is defined as:

$$\langle \Psi_L|\hat{\psi}\rangle = \frac{1}{2} \int \left(\Psi_L^* \hat{\psi} + \Psi_L \hat{\psi}^\dagger \right) dx$$

where we use the mean-field soliton with an adjustable phase shift as the local oscil-

lator profile, $\Psi_L = \Psi_0 e^{i\theta}/P$. By varying the phase of the homodyne detection, θ, we can determine the minimum value of the squeezing ratio of the quadrature component of the quantum field. The result of the calculations of $R(t)$ for the gap soliton near the bottom edge of the spectral gap is presented in Fig. 3.8 by a solid curve.

The optimal squeezing ratio for gap solitons can be compared with that for a conventional NLS soliton coinciding with the soliton envelope $F(x)$ and evolving in a lattice-free anomalous diffraction regime (dashed line in Fig. 3.8). The NLS soliton of the same envelope as the gap state is only weakly quadrature squeezed during propagation due to the nonlinearity of the matter-wave, whereas the gap soliton shows enhanced quantum noise squeezing. In contrast, the near-band-edge envelope approximation of Eq. (3.13) (dot-dashed line in Fig. 3.8) provides a good estimate for soliton squeezing in the initial stage of evolution.

To understand the band-gap effect on the quantum fluctuation of matter-wave gap solitons, we analyze the number correlations between different spectral components of the gap soliton induced by its nonlinear evolution. The intra-soliton correlation coefficients, C_{ij}, are found by calculating the normally-ordered covariance,

$$C_{ij} \equiv \frac{\langle : \Delta\hat{n}_i \Delta\hat{n}_j : \rangle}{\sqrt{\Delta\hat{n}_i^2 \Delta\hat{n}_j^2}} \ , \tag{3.14}$$

where $\Delta\hat{n}_j$ is the atom-number fluctuation in the j-th slot Δs_j in the spatial ($s = x$) or momentum ($s = k$) domain:

$$\Delta\hat{n}_j = \int_{\Delta s_j} d\,s [\Psi_0(t,s)\hat{\psi}^\dagger(t,s) + \Psi_0^*(t,s)\hat{\psi}(t,s)],$$
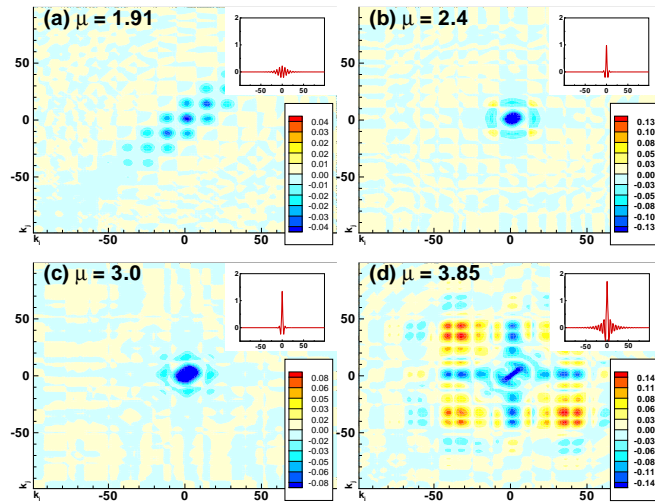
FIGURE 3.9: Quantum correlation spectra in the *spatial* (x)-domain for gap solitons at different points within the gap. Insets show the corresponding components of solitons in the x-domain. For distinctness, all figures are plotted with the different set of correlation densities.

The corresponding number correlation spectra in the *spatial* (x)-domain for gap solitons at different points within the gap are shown in Figs. 3.9 (a-d), respectively. Compared to the well-known correlation spectrum of NLS soliton, the near-band-edge gap soliton has enlarged and discrete correlation pattern "shaped" by the Bragg scattering of the matter-wave on the periodic potential. And in the *momentum* domain NLS soliton displays the well-known symmetric correlation pattern with the noisy, strongly correlated outer regions of the soliton spectrum. For this reason, an efficient number squeezing of NLS solitons can be produced by spectral filtering that removes the noisy spectral components [49]. On the contrary, the correlation spectrum of a near-band-edge gap soliton displays a periodic pattern with regions of strong anti-correlations at the Bragg condition, $k = \pm(2m + 1)$ (m is an integer). This ensures
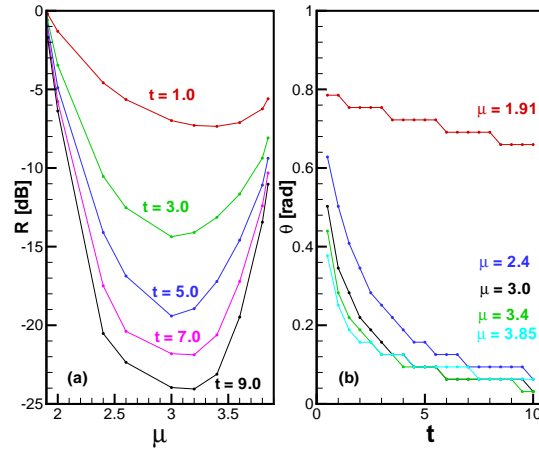
FIGURE 3.10: (a)Optimal squeezing ratios, R, for gap solitons with different chemical potentials, μ, at different time. (b) Time evolution of the phase in the homodyne detection for the optimal squeezing ratios at different values of chemical potentials within the gap.

enhanced number squeezing of the BEC soliton *without* additional spectral filtering.

When the chemical potential of the gap soliton moves away from the band edge, the envelope approximation (3.13) becomes invalid. In Fig. 3.10(a), we show the dependence of the optimal squeezing ratios of gap solitons at different chemical potentials inside the gap for different times. Towards the middle of the gap, the squeezing ratio improves with the chemical potential as the peak density of the gap soliton and the nonlinear interaction is increasing. It must be emphasized that near the band edge the quantum noises of gap solitons is squeezed in the quadrature field component, Fig. 3.10 (b). But like amplitude-squeezed fiber Bragg grating solitons [64], gap solitons become atom-number squeezed, $\theta \approx 0$, when their chemical potentials move toward the band gap (θ is not exactly zero for we don't use an optimal profile

for the local oscillator.) For a fixed time (say at $t = 5$) and varying chemical potential, the best squeezing occurs in the middle of the gap, at $\mu = 3.0$. Analysis of the number correlation structure reveals that the gap soliton in the middle of gap is entirely composed of strongly localized, weakly anti-correlated components [Fig. 3.9 (b)], which assists the atom number squeezing. However, near the top edge of the gap, the localization of the gap soliton degrades due to resonance with the Bloch state at the corresponding edge, and strongly correlated, noisy components associated with the periodic Bloch wave structure start to dominate in the soliton spectrum [Fig. 3.9 (d)]. Subsequently, the squeezing is reduced on that edge of the spectral gap. In between, the balance of spectral filtering induced by the periodic potential and the delocalization of Bloch wave states makes the squeezing ratio of gap soliton to a minimum value [Fig. 3.9 (c)].
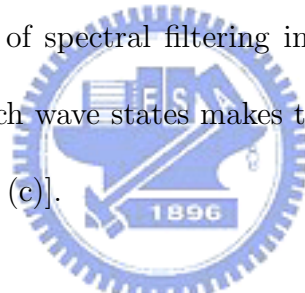
3.4. Summary

In summary, we have developed a general quantum theory for bi-directional non-linear optical pulse propagation problems and have especially used it to study the squeezing phenomena of fiber Bragg grating solitons. It has been shown for the first time that the output FBG soliton pulses will get amplitude squeezed automatically. The squeezing ratio of the FBG solitons exhibits interesting relation with the fiber grating length as well as with the intensity of the input pulse. The squeezing ratio saturates after a certain grating length and the optimal squeezing ratio occurs when

the intensity of the FBG soliton is slightly large than that of the fundamental soliton. With the use of apodized FBGs, we also find that one can compress the FBG solitons and enhance its squeezing ratio simultaneously, as long as the soliton pulses evolve adiabatically. To actually measure the quantum fluctuations of the fiber Bragg grating solitons experimentally, we propose to use a time-gating device to block out other smaller multiple transmitted pulses and only directly detect the first transmitted pulse from the grating.

We also have investigated the effect of the periodic potential on quantum fluctuations of gap solitons in repulsive BEC confined by an optical lattices. We have revealed that the quantum correlation spectra of gap solitons show discrete and delocalized patterns in the *spatial* domain which are introduced by the periodic nature of Bloch states. This property of intra-soliton quantum correlations causes the enhanced squeezing of gap states compared the envelope solitons described by the NLS equation. And we find that gap soliton gets quadrature squeezed near the band edge and atom number squeezed inside the band gap. We would like to emphasize that the basic results of our analysis can be useful in the study of the bandgap effects on the quantum squeezed states in other fields, such as quantum optics and gap solitons in photonic crystals.

CHAPTER 4

Soliton Entanglement

4.1. Introduction

Quantum-noise squeezing and correlations are two key quantum properties that can exhibit completely different characteristics when compared to the predictions of the classical theory. Almost all the proposed applications to quantum measurements and quantum information treatment utilize either one or both of these properties. In particular, solitons in optical fibers have been known to serve as a platform for demonstrating macroscopic quantum properties in optical fields, such as quadrature squeezing [33, 34, 36, 37, 62, 63], amplitude squeezing [49, 64], and both intra-pulse and inter-pulse correlations [58, 65].

Recently, experimental progress in demonstrating various quantum information processes by using two-mode squeezed states in optical solitons has been reported, see Refs. [66, 67, 68] and references therein. In previous works, continuous-variable entangled beams have been generated by letting two squeezed fields (squeezed vacuum states [69], or amplitude-squeezed fields [70]) interfere through a beam splitter, which mathematically acts as the Hadamard transformation. By utilizing the continuous EPR-like correlations of optical beams, one can also realize quantum-key distribu-

tions [67] and entanglement swapping [68]. Thanks to these successful applications, squeezed states become essential for generating entangled continuous-variable quantum states, and play an important role in the study of the quantum-information processing.

It has been demonstrated that two independent squeezed pulse states can be simultaneously generated by using optical solitons in the Sagnac fiber loop configuration [66]. An EPR pulse source can be obtained by combining the two output pulse squeezed states by means of a 50:50 beam splitter. In contrast to this known method for achieving the entanglement, in the first part of this **Chapter** we propose simple schemes for generating continuous-variable entangled states through *continuous interaction* of two solitons, not collision, in single-mode and bimodal (two-component) systems, *without* using beam splitters. The quantum interaction of two time-separated solitons in the same polarization is described by the quantum nonlinear Schrödinger equation (NLSE), and in the bimodal system, including two polarizations, it is described by a system of coupled NLSEs. The photon-number correlation between the two solitons can be numerically calculated by using the *back-propagation method* [16]. In addition to the transient multimode correlations induced by cross-phase modulation [65], we also find nearly maximum photon-number entanglement in the soliton pair. By controlling the initial separation of the two solitons, one can achieve a positive quantum correlation with the correlation parameter taking values close to 1.

In the NLSE model, adjacent temporal solitons attract or repel each other, de-

pending on the phase shift between them [71]. In the cases when the potential inter-action force between the solitons can be balanced by additional effects, such as those induced by small loss and gain terms in a perturbed cubic [72, 73] or quintic NLSE [74, 75, 76, 77, 78] [which actually turns the NLSE equation into a complex Ginzburg-Landau equation (CGLE)], or the polarization structure of the optical field, described by the coupled NLSEs [79, 80, 81], bound states of solitons have been predicted. Recently, formation of stable double-, triple-, and multi-soliton bound states (*trains*, in the latter case) has been observed experimentally in various passively mode-locked fiber-ring laser systems [82, 83, 84], which offers potential applications to optical telecommunications. Formation of "soliton crystals" in nonlinear fiber rings has been predicted too [85].
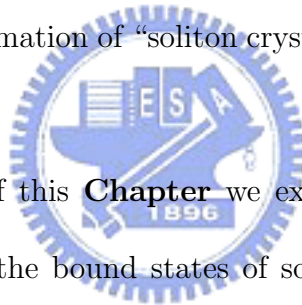
In the second part of this **Chapter** we extend the idea of *interaction induced soliton entanglement* to the bound states of solitons in the CGLE. We find strong quantum-perturbation correlations between the bound solitons, despite the fact the dissipative nature of the model will indeed prevent observation of the squeezing of the quantum fluctuations around the bound solitons in the fiber-ring lasers described by the CGLE. Multimode quantum-correlation spectra of the bound-soliton pairs show patterns significantly different from those for two-soliton configurations in the conservative NLSE. We also find a similarity in the photon-number correlations between the stable bound-soliton pairs and multi-soliton trains. These photon-number-correlated soliton pairs and trains may offer new possibilities to generate multipartite entangled

sources for applications to quantum communications and computation.

Since the non-conservative terms in the CGLE may be superficially considered as detrimental to the observation of quantum fluctuations of fiber solitons. In the last part of this **Chapter**, we show that the possibility to achieve squeezing of atomic solitons paves the way to creation of entangled macroscopic coherent states in BEC interference experiments. However, optical lattices also offer an alternative possibility for entanglement production. It is known that the optical lattice supports stationary states in the form of bound gap soliton pairs [40, 86]. The nonlinear interaction between solitons in a pair could induce quantum entanglement and hence nonseparability of the bound state. This entanglement can potentially be exploited in BEC atom number detection by implementing analogs of quantum nondemolition measurements based on entangled pairs of optical solitons [87]. Potential advantage of gap solitons compared to the lattice-free atomic solitons is the long-lived nature of the bound states which are pinned by the lattice and do not break-up as a result of evolution. Hence strong interaction-induced atom-number correlations can develop between the atomic wavepackets.

4.2. Interaction induced soliton entanglement, NLSE model

Neglecting loss and higher-order effects, which are immaterial for the experimentally relevant range of the propagation distance z, temporal solitons in optical fibers
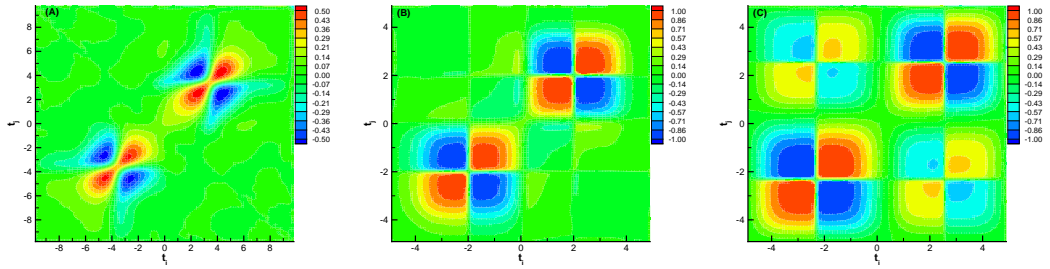
FIGURE 4.1: The pattern of time-domain photon-number correlations, C_{ij}, of two interacting out-of-phase solitons, with $\theta = \pi/2$, $\rho = 3.5$, and $\gamma = 1.0$ in Eq. (4.1). The propagation distance is $z = 6$ (A), 30 (B), and 50 (C), in the normalized units. The width of the time slots is $\Delta t = 0.1$. Note the difference in the bar-code scales in the panels (A) and (B), (C).

are described by the NLSE in the normalized form,

$$ iU_z + \frac{1}{2}U_{tt} + |U|^2U = 0, $$

where t is the retarded time [71]. The input profile of the soliton pair is taken as

$$ U(z,t) = \text{sech}(z, t + \rho) + \gamma \, \text{sech}(z, t - \rho)e^{i\theta}, \tag{4.1} $$

where γ, θ, and 2ρ are, respectively, the relative amplitude, phase and separation of the solitons. If $\theta = 0$ (the in-phase pair), the two solitons will form a breather, periodically colliding in the course of the propagation. Otherwise, they move apart due to repulsion between them. The interaction between the solitons is produced by the overlap of the "body" of each soliton with an exponentially decaying "tail" of the other one. A detailed account explaining the tail-mediated interaction in the NLSE with the instantaneous cubic (Kerr) nonlinearity can be found in the review [88].

In Fig. 4.4, we display the result of evaluation of the time-domain photon-number

correlations for the out-of-phase ($\theta = \pi/2$) two-soliton pair. The correlation coefficients, which are defined through the normally ordered covariance,

$$C_{ij} \equiv \frac{\langle : \Delta\hat{n}_i \Delta\hat{n}_j : \rangle}{\sqrt{\Delta\hat{n}_i^2 \Delta\hat{n}_j^2}} \ , \tag{4.2}$$

were calculated by means of the above-mentioned back-propagation method [16]. In Eq. (4.2), $\Delta\hat{n}_j$ is the photon-number fluctuation in the i-th slot Δt_i in the time domain,

$$\Delta\hat{n}_i = \int_{\Delta t_i} d\,t [U(z,t)\Delta\hat{U}^{\dagger}(z,t) + U^*(z,t)\Delta\hat{U}(z,t)],$$

where $\Delta\hat{U}(z,t)$ is the perturbation of the quantum-field operator, $U(z,t)$ is the classical unperturbed solution, and the integral is taken over the given time slot. As could be intuitively expected, nonzero correlation coefficients are found solely in the diagonal region of the spectra (*intra-pulse correlations*) if the interaction distance is short, as shown in Fig. 4.4(A). As the interaction distance increases, *inter-pulse correlations* between the two solitons emerge and grow, as shown in Figs. 4.4(B) and (C).

In addition to the time-domain photon-number correlation pattern, we have also calculated a photon-number *correlation parameter* between the two interaction solitons, as

$$C_{12} = \frac{\langle : \Delta\hat{N}_1 \Delta\hat{N}_2 : \rangle}{\sqrt{\Delta\hat{N}_1^2 \Delta\hat{N}_2^2}}.$$

Here $\Delta\hat{N}_{1,2}$ are the perturbations of the photon-number operators of the two solitons, which are numbered (first and second) according to their position in the time domain.
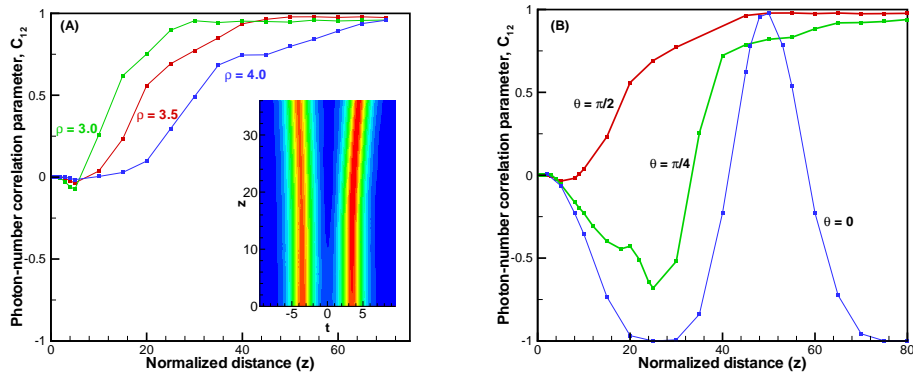
FIGURE 4.2: The photon-number correlation parameter C_{12} for the soliton pair with different values of the separation ($\rho = 3.0$, 3.5, 4.0, while $\theta = \pi/2$ and $\gamma = 1.0$) in (A), and different values of the relative phase ($\theta = 0$, $\pi/4$, $\pi/2$, while $\rho = 3.5$ and $\gamma = 1.0$) in (B). The inset in (A) shows the evolution of the interaction solitons by means of contour plots.

In Fig. 4.5 (A), we show the coefficient C_{12} for the soliton pair (4.1) with the initial relative phase $\theta = \pi/2$, equal amplitudes ($\gamma = 1.0$), and different values of the separation ρ. At the initial stage of the interaction, the photon-number fluctuations are uncorrelated between the solitons, $C_{12} \approx 0$. After passing a certain distance, the photon-number correlations between the two solitons gradually build up, and the pair may become a nearly maximum-positive-correlated one. In accordance with the fact that the interaction between the solitons, which gives rise to the correlations, is mediated by their exponentially decaying tails, the propagation distance needed to achieve the maximum positive photon-number correlation decreases with the initial separation between the solitons.

On the other hand, one can fix the initial separation but vary the initial relative
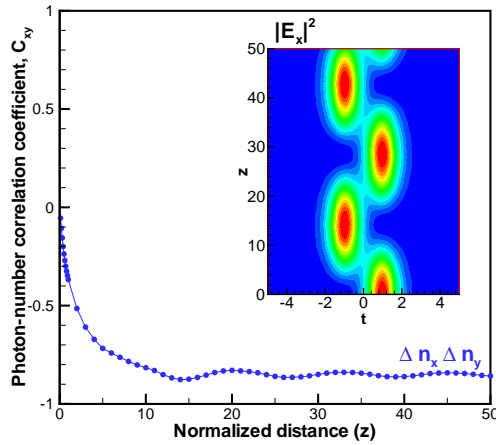
FIGURE 4.3: The photon-number correlation coefficient of interacting vectorial solitons. The inset displays the evolution of the x-component of the classical field.

phase between the solitons. For this case, the results are shown in Fig. 4.5(B). Similar to the case of soliton-soliton collisions [65], the photon-number correlation coefficient oscillates, as a function of the propagation distance, with the period equal to that of the two-soliton breather, if the solitons are, initially, in-phase. Note that in the case which may be regarded as intermediate between the in-phase and out-of-phase ones, $\theta = \pi/4$, the correlation coefficient first becomes negative, and then positive.

Unless $\theta = 0$ (when the two solitons form a quasi-bound state in the form of a breather), the two solitons belonging to the initial configuration (4.1) will separate as a result of the propagation. Therefore, the interaction between them eventually vanishes, and thus the photon-number correlation coefficient may saturate before it has a chance to reach the value corresponding to the total positive correlation, which is clearly seen in the inset to Fig. 4.5(A).

The time-division entangled soliton pair in the single-mode system, considered above, can be separated with an optical switch. Since the actual time separation between the two solitons is, typically, on the order of a few picoseconds, a lossless ultrafast optical switch will be required for the actual implementation of the scheme. The experimental difficulties can be greatly reduced if another scheme is used, which utilizes vectorial solitons in two polarizations. The model is based on the well-known system of coupled NLSEs [71],

$$i\frac{\partial U}{\partial z} + \frac{1}{2}\frac{\partial^2 U}{\partial t^2} + A|U|^2 U + B|V|^2 U = 0, \tag{4.3}$$

$$i\frac{\partial V}{\partial z} + \frac{1}{2}\frac{\partial^2 V}{\partial t^2} + A|V|^2 V + B|U|^2 V = 0. \tag{4.4}$$

Here U and V are the fields in orthogonal circular polarizations, A and B being the self-phase- and cross-phase-modulation coefficients, respectively, with the relation $A : B = 1 : 2$ in the ordinary optical fibers [71]. We take the following initial configuration for the soliton pair [cf. Eq. (4.1)],

$$U = \mathrm{sech}(t + t_1) + \mathrm{sech}(t - t_1), \tag{4.5}$$

$$V = \mathrm{sech}(t + t_1) - \mathrm{sech}(t - t_1). \tag{4.6}$$

Using the methods for the analysis of the classical vectorial solitons developed in Refs. [79, 80, 81, 89], we calculated the respective quantum fluctuations and the photon-number correlations numerically. It should be noted the total intensity of the vectorial solitons, defined in terms of the circular polarizations, remains unchanged during the propagation, but the intensities of the linearly-polarized (x- and y-) com-

ponents, $E_x = (U+V)/\sqrt{2}$ and $E_y = -i(U-V)/\sqrt{2}$, evolve periodically, as shown in the insert of Fig. 4.3. In this figure, we display the evolution of the photon-number correlation between the x- and y- components of the vectorial solitons, which are originally uncorrelated, and then become negatively correlated. It should be stressed that if one uses the polarization fields proper, U and V, as the projection basis, there are no strong photon-number correlations between these two fields. It is necessary to employ an appropriate basis – for example, the polarizations E_x and E_y in the present case – to identify highly photon-number-correlated pairs.

4.3. Entangled bound-state of solitons in CGLE model

Multiple-pulse generation in the passively mode-lock fiber lasers is quite accurately described by the quintic CGLE (which is written here in a normalized form),

$$iU_z + \frac{D}{2}U_{tt} + |U|^2U = i\delta U + i\epsilon|U|^2U + i\beta U_{tt} + i\mu|U|^4U - \nu|U|^4U, \qquad (4.7)$$

where U is the local amplitude of the electromagnetic wave, z is the propagation distance, t is the retarded time, and D corresponds to anomalous dispersion $(+1)$ or normal dispersion (-1). Besides the group-velocity dispersion (GVD) and Kerr effect, which are accounted for by conservative terms on the left-hand-side of Eq. (4.7), the equation also includes the quintic correction to the Kerr effect, through the coefficient ν, and non-conservative terms (the coefficients δ, ϵ, μ, and β account for the linear, cubic, and quintic loss or gain, and spectral filtering, respectively).

Following the known approach to the investigation of bound- soliton states [72, 74, 77], the corresponding solution to Eq. (4.7) is sought for in the form

$$U(z,t) = \sum_{j=1}^{N} U_0(z, t + \rho_j)e^{i\theta_j},$$

where U_0 is a single-soliton solution, and ρ_j and θ_j are the coordinates separation and phases of the individual solitons. Through the balance between the gain and loss, in-phase and out-of-phase bound-soliton pairs may exist in the anomalous-GVD regime, which is described by Eq. (4.7).

We compute quantum fluctuations around these pairs by dint of a numerically implemented *back-propagation method* [16], which may be summarized as follows. First of all, one replaces the classical function $U(z,t)$ in Eq. (4.7) by the quantum-field operator variable, $\hat{U}(z,t)$, which satisfies the equal-coordinate Bosonic commutation relations. Next, the equation is linearized around the classical solution through the substitution of $\hat{U}(z,t) = U_0 + \hat{u}(z,t)$, assuming large photon numbers in the solitons. Then, a zero-mean additional noise operator, $\hat{n}(z,t)$, is introduced, to make the quantum-perturbation fields in the linearized equation satisfy the Bosonic communication relations (see Ref. [90] for more details). It should be emphasized that the magnitude of the noise level calculated herewith represents the *minimum* quantum noise (in the nonconservative model), i.e., a lower limit required by the fundamental principles of quantum mechanics.

In Fig. 4.4, we display the comparison of the *time-domain* photon-number correlations for the two- soliton configuration in the conservative cubic NLSE model (a),
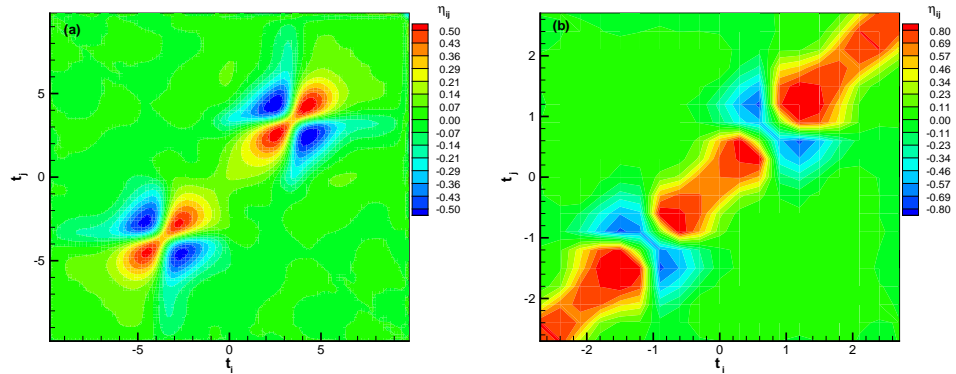
FIGURE 4.4: A typical pattern of the time-domain photon-number correlations, η_{ij}, for an out-of-phase two- soliton state in the cubic NLSE model (a), after 6 normalized propagation distance; and for an in-phase two- soliton bound state in the CGLE model (b), after 0.5 normalized propagation distance.

and an in-phase two-soliton bound state in the CGLE model (b). In the NLSE model, there are two isolated patterns for the two-solitons configuration, corresponding to the *intra-pulse correlations* of individual solitons, see Fig. 4.4(a). However, it is obvious from Fig. 4.4(b) that there is a band of strong correlations between the two bound solitons in the quantum CGLE model. This strong-correlation band can be explained by the interplay between the nonlinearity, GVD, gain, and loss in the model. The balance between these features not only supports the classical stable bound state of the soliton, but also causes strong correlations between their quantum fluctuations.

In addition to the time-domain photon-number correlation pattern, we have also calculated a photon-number *correlation parameter* between the two bound solitons. Figure 4.5 shows the evolution of the photon-number correlation parameter in the two-soliton bound state. Initially, the classical laser statistics (coherent state) is assumed
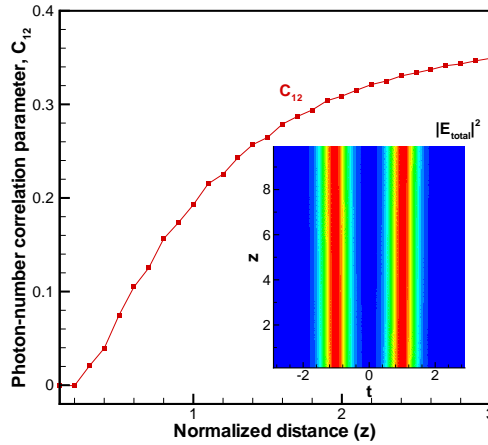
FIGURE 4.5: The evolution of the photon-number correlation parameter, C_{12}, for two bound in-phase solitons. The computations were carried out for the following values of parameters in the CGLE: $D = 1$, $\delta = -0.01$, $\epsilon = 1.8$, $\beta = 0.5$, $\mu = -0.05$, and $\nu = 0$. The inset illustrates the stability of the underlying classical solution for the two- soliton bound state, by means of contour plots.

for each soliton, without correlation between them, $C_{12} \approx 0$. In the course of the evolution, the photon-number correlation between the two bound solitons gradually increases to positive values of C_{12}, and eventually it saturates about $C_{12} = 0.36$. The inter- soliton correlation is induced and supported by the interaction between the solitons. In a conservative system, such as the NLSE model, nearly perfect photon-number correlations can be established if the interaction distance is long enough [94]. In a non-conservative system, such as in the CGLE model, the action of the filtering, linear and nonlinear gain, and losses lead to the saturation of the photon-number correlation parameter. Thus, while the large quantum fluctuations in the output bound-soliton pair will eclipse any squeezing effect, the correlated fluctuations
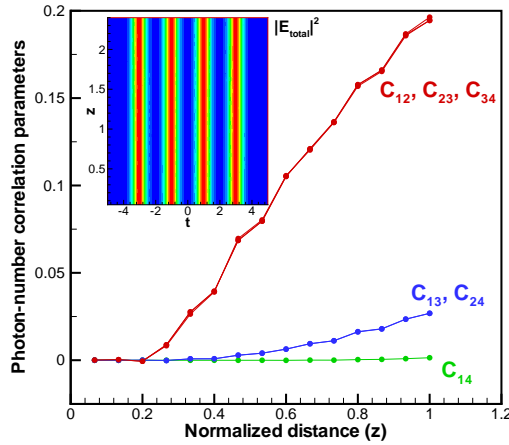
FIGURE 4.6: The evolution of the photon-number correlation parameters, C_{ij}, for a bound complex (train) of four in-phase solitons in the CGLE model. The soliton's number $(1, 2, 3, 4)$ runs from left to right. Parameters are the same as in the case shown in Fig. (4.5). The inset demonstrates the stability of the underlying classical solution for the four-soliton train.

between the bound soliton are predicted to be observable.

The approach elaborated here for the study of the quantum-noise correlations between two bound solitons can be easily extended to multi-soliton bound states (soliton trains). Figure 4.6 shows the photon-number correlation parameters, C_{ij}, in a train of four equal-separated in-phase bound solitons. Again, the photon-number fluctuations are initially uncorrelated between the solitons. As could be expected, we find that soliton pairs with equal separations have practically identical correlation coefficients, i.e. , $C_{12}(z) \approx C_{23}(z) \approx C_{34}(z)$, and $C_{13}(z) \approx C_{24}(z)$. Obviously, when the interaction between the soliton trains is stronger, as the separation between them is smaller, the values of the correlation parameter are larger. Note that the correlation
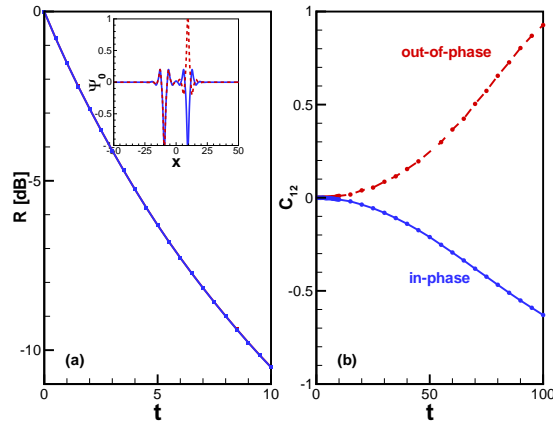
FIGURE 4.7: (a) Optimal squeezing ratios of the in-phase (inset, solid) and out-of-phase (inset, dashed) bound states of gap solitons at $V_0 = 4.0$ and $\mu = 2.5$. The two curves completely overlap. (b) Atom number correlation parameter C_{12} for the in-phase (solid line) and out-of-phase (dashed line) gap-soliton pairs.

coefficient for the most separated pair in the train, C_{14}, grows very slowly with z. Eventually, all of the curves of $C_{ij}(z)$ saturate due to the dissipative effects in the CGLE model.

4.4. Entangled bound gap soliton pairs

Although in the lattice-free NLSE model, no bound-state solutions of soliton pairs exist due to the interaction potential between them. But with help of periodic potentials, gap solitons support in-phase and out-of-phase bound states solutions, as shown in Fig. 4.7 for the case in the middle of spectral gap. These states contain the same number of atoms for the same μ, which equals to exactly twice the number of atoms in a single soliton.

Remarkably, the *internal* noise correlation properties are the same for both pairs, which results in their identical optimal number squeezing ratio (see Fig. 4.7 (a)). Soliton entanglement can be quantified by inter-soliton atom number correlations which can be calculated according to Eq. (4.2), with $\Delta \hat{n}_{i,j}$ being perturbations of the atom number operator of two solitons, and indices $\{i, j\} = \{1, 2\}$ numbering individual solitons. The evolution of the correlation parameter C_{12} shows dramatic difference between the in- and out-of-phase soliton pairs. As follows from Fig. 4.7 (b), the atom number correlation parameter for the in-phase soliton pair is negative while it is positive for the out-of-phase pair. The difference in the entanglement behavior can be understood by examining the interaction energy of the solitons in the pair $E_{12} = \int E_{12}(x)dx$, with the energy density defined as:

$$E_{12} = \sum_{i \neq j} \frac{1}{2} \psi_i \frac{d^2}{dx^2} \psi_j + \overline{V(x)\psi_i\psi_j} + 3|\psi|_i^2|\psi|_j^2 + 4\psi_i^3\psi_j.$$

Interaction energy, E_{12} depends on overlapping tail structure of the stationary profiles $\psi_{1,2}(x)$ corresponding to mean-field solitons Ψ_0. This quantity is small but positive, $E_{12}^{\text{out}} = 3.4 \times 10^{-2}$, for the out-of-phase soliton pair in Fig. 4.7 (a, inset), and negative, $E_{12}^{\text{in}} = -3.2 \times 10^{-2}$, for the in-phase pair. This results in positive and negative atom-number correlation parameter for the respective pairs. Small difference in moduli of the interaction energies is responsible for the slight asymmetry in correlations development seen in Fig. 4.7 (b). As a result, longer evolution times are required for the development of maximum atom number correlations between the solitons in an in-phase pair.

4.5. Summary

In this **Chapter**, we have studied the quantum photon-number correlations induced by the interactions between two solitons, mediated by their tails, from the time-division, polarization-division pairs, bound soliton states in CGLE model, and bound gap-soliton pairs. In the first two cases of lattice-free NLSE model, using the pair with suitable initial separation and relative phase, one can generate positive or negative photon-number-correlated soliton pairs. An ultrafast optical switch will be needed to separate the two entangled solitons into different channels for the time-division case. On the other hand, by using the vectorial solitons with two polarization components, pairs with negative photon-number correlations between the solitons can be generated. For this case, a simple polarization beam splitter will be sufficient to separate the two entangled solitons.

We also have extended the concept of quantum fluctuation around classical optical solitons to the non-conservative model based on the CGLE with the cubic-quintic nonlinearity. Applying the known back-propagation method to the linearized equations that govern the evolution of the fluctuations, we have numerically calculated the photon-number correlations and the effective correlation coefficient for pairs of bound solitons, as well as for multi-soliton bound complexes (trains). We have demonstrated that, unlike the two-soliton configuration in the conservative NLSE model, there is a band of strong quantum correlation in the bound-soliton pair. While the dissipative

effects in the CGLE model will totally suppress the generation of squeezed states from bound solitons, as one might expect, there still exists a certain degree of correlations between photon-number fluctuations around the stable bound-soliton pairs and trains.

Finally, we shown that nonlinear interaction of gap solitons in dynamically stable bound states can produce strong soliton entanglement. Furthermore, we show that the existence of dynamically stable bound states of gap solitons provides a favorable environment for generation of entangled soliton pairs. Such photon-number-correlated soliton pairs feature unique entanglement properties, which may offer new possibilities for applications to quantum communications and computation. The applications will be considered as future research projects. And it shall be very interesting to see if one can actually verify the theoretical predictions experimentally.

CHAPTER 5

Conclusions

In conclusion, in this dissertation we have studied the quantum optical phenomena in photonic crystals (PhCs) including the atom-light interactions and the nonlinear soliton waves. Squeezing effects are predict to be observed in the fluorescence spectra [91], Bragg solitons [64, 92], and gap solitons [93]. New schemes for generating entangled soliton sources through the soliton interaction are proposed and analyzed in details [90, 94].

In the part of atom-light interaction, we have developed a new formulation to calculate the fluorescence spectrum with non-Markovian photon-atom interactions, and have successfully applied it to the case of a single two-level atom embedded in a photonic bandgap crystal. By introducing the Liouville operator expansion, we can overcome some of the difficulties caused by the non-Markovian nature of the problem due to the non-uniform distribution of the photon states in the photonic bandgap crystals. The calculated results for resonance pumping have indicated that the resonance fluorescence spectra near a photonic bandgap can exhibit interesting behaviors including the suppression and enhancement of the Mollow's triplet peaks, and the squeezing phenomena in the in-phase quadrature spectra.

In the part of nonlinear photonic crystals, we have developed a general quantum

theory for bi-directional nonlinear optical pulse propagation problems and have used it to calculate the squeezing ratio of the fiber Bragg grating (FBG) solitons in one-dimensional PhCs for the first time. If the pulse shape of the local oscillator is assumed to be the same as the pulse shape of the output pulse, we find that the output pulses can get amplitude squeezed and the squeezing ratio exhibits interesting relations with the fiber grating length as well as with the intensity of the input pulse. The same idea is applied to the matter-wave gap solitons in a repulsive Bose-Einstein condensate loaded into a one-dimensional optical lattices. By employing a linearized quantum theory we find that quantum noise squeezing of gap solitons, produced during their evolution, is enhanced when compared with the atomic solitons in a lattice-free case, due to the intra-soliton structure of quantum correlations induced by the Bragg scattering in the periodic potential.

Like semiconductor crystals, we can use the defects in PhCs to control the flow of the light, such as the cases in waveguides and micro-cavities. For one-dimensional PhCs, the manufacturing technologies and the design algorithms for various types of fiber Bragg gratings have been very mature and have already been applied to design very complicated structures. Based on our previous studies of solitary waves propagating in FBGs, one of our next works is to investigate the solitary waves propagating in non-uniform FBGs with/without defects. The quantum effects of defects in nonlinear PhCs have not yet been studied in the literature.

The results of this thesis can also be applied to the generation of nonclassical

lights from multi-stable solitons in the presence of higher-order nonlinearity, as well as from multi-dimensional solitons. In the later case, the higher order nonlinearity is necessary to prevent collapse. These nonclassical output sources in multi-dimensions may also be useful for processing continuous-variable quantum information.

For the one-dimensional problem, one can use the inverse scattering methods (ISM) to inversely design the grating structure. The quantum inverse scattering methods for one-dimensional problems have also been well-developed. However, how to apply the ISM to high-dimensional PhCs is still an open problem. From the numerical point of view, solving the problems of two or three-dimensional PhCs is not an easy work, too. Examples of high-dimensional nonlinear photonic crystals have been reported in the literature recently. Finding an efficient numerical method to study the quantum effects of these high-dimensional nonlinear photonic crystals is also one of our further challenges.
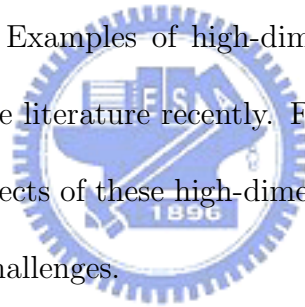
BIBLIOGRAPHY

[1] E. Yablonovitch, "Inhibited spontaneous emission in solid-state physics and electronics," *Phys. Rev. Lett.* **58**, 2059 (1987).

[2] S. John, "Strong localization of photons in certain disordered dielectric superlattices," *Phys. Rev. Lett.* **58**, 2486 (1987).

[3] E. M. Purcell, "Spontaneous emission probabilities at radio frequencies," *Phys. Rev.* **69**, 681 (1946).

[4] S. John and J. Wang, "Quantum electrodynamics near a photonic band gap: photon bound states and dressed atoms," *Phys. Rev. Lett.* **64**, 2418 (1990).

[5] S. John and T. Quang, "Spontaneous emission near the edge of a photonic band gap," *Phys. Rev. A* **50**, 1764 (1994).

[6] S.-Y. Zhu, H. Chen, and H. Huang, "Quantum interference effects in spontaneous emission from an atom embedded in a photonic band gap structure," *Phys. Rev. Lett.* **79**, 205 (1997).

[7] E. Paspalakis and P. L. Knight, "Phase control of spontaneous emission," *Phys. Rev. Lett.* **81**, 293 (1998).

[8] E. Paspalakis, N. J. Kylstra, and P.L. Knight, "Transparency near a photonic band edge," *Phys. Rev. A* **60**, R33 (1999).

[9] M. Florescu and S. John, "Single-atom switching in photonic crystals," *Phys. Rev. A* **64**, 033801 (2001).

[10] A. B. Aceves, and S. Wabnitz, "Self-induced transparency solitons in nonlinear refractive periodic media," *Phys. Lett. A* **141**, 37 (1989).

[11] S. F. Mingaleev and Yu. S. Kivshar, "Self-trapping and stable localized modes in nonlinear photonic crystals," *Phys. Rev. Lett.* **86**, 5474 (2001).

[12] R. Slusher and B. Eggleton, Eds, *"Nonlinear Photonic Crystals,"* (Springer-Verlag, Berlin, 2003).

[13] O. Zobay, S. Pötting, P. Meystre and E.M. Wright, "Creation of gap solitons in Bose-Einstein condensates," *Phys. Rev. A* **59,** 643 (1999).

[14] E. A. Ostrovskaya and Yu.S. Kivshar, "Matter-wave gap solitons in atomic band-gap structures," *Phys. Rev. Lett.* **90**,160407 (2003).

[15] B. Eiermann, Th. Anker, M. Albiez, M. Taglieber, P. Treutlein, K.-P. Marzlin, and M. K. Oberthaler, "Localization of two-component Bose-Einstein condensates in optical lattices," *Phys. Rev. Lett.* **92**, 230401 (2004).

[16] Y. Lai and S.-S. Yu, "General quantum theory of nonlinear optical-pulse propagation," *Phys. Rev. A* **51**, 817 (1995).

[17] R. Loudon, *"The quantum theory of light,"* 2nd ed. (Oxford University Press, New York, 1983).

[18] R. R. Mollow, "Power spectrum of light scattered by two-level systems," *Phys. Rev.* **188**, 1969 (1969).

[19] C. Cohen-Tannoudji, in *"Frontiers in Laser Spectroscopy,"* edited by R. Balian, S. Haroche, and S. Liberman (North-Holland, New York, 1977.)

[20] H. J. Kimble, M. Dagenais, and L. Mandel, "Photon antibunching in resonance fluorescence," *Phys. Rev. Lett.* **39**, 691 (1977).

[21] F. Y. Wu, S. Ezekiel, M. Ducloy, and B. R. Mollow, "Observation of amplification in a strongly driven two-level atomic system at optical frequencies," *Phys. Rev. Lett.* **38**, 1077 (1977).

[22] D. F. Walls and P. Zoller, "Reduced quantum fluctuations in resonance fluorescence," *Phys. Rev. Lett.* **47**, 709 (1981).

[23] L. Mandel, "Squeezed states and sub-poissonian photon statistics," *Phys. Rev. Lett.* **49**, 136 (1982).

[24] M. J. Collett, D. F. Walls, and P. Zoller, "Spectrum of Squeezing in resonance fluorescence," *Opt. Comm.* **52**, 145 (1984);

[25] D. F. Walls and G. J. Milburn, *"Quantum Optics,"* 2nd ed. (Springer-Verlag, Berlin, 1984.)

[26] Z. H. Lu, S. Bali, and J. E. Thomas, "Observation of squeezing in the phase-dependent fluorescence spectra of two-level atoms," *Phys. Rev. Lett.* **81**, 3635 (1998).

[27] M. Lewenstein, J. Zakrzewski, and T. W. Mossberg, "Spontaneous emission of atoms coupled to frequency-dependent reservoirs," *Phys. Rev. A* **38**, 808 (1988).

[28] S. Y. Zhu, Y. Yang, H. Chen, H. Zheng, and M. S. Zubairy, "Spontaneous radiation and lamb shift in three-dimensional photonic crystals," *Phys. Rev. Lett.* **84**, 2136 (2000).

[29] Y. Yamamoto, and A. İmamoḡlu *"Mesoscopic Quantum Optics,"* (John Wiley & Sons, Inc. 1999).

[30] P. Zhou and S. Swain, "Enhancement of squeezing in the resonance fluorescence of a laser-dressed atom with finite-bandwidth cavity-field excitation," *Phys. Rev. A* **59**, 1603 (1997).

[31] Yu. S. Kivshar and G. P. Agrawal, *"Optical Solitons: From Fibers to Photonic Crystals,"* (Academic, San Diego, 2003).

[32] B. J. Eggleton, R. E. Slusher, C. M. de Sterke, P. A. Krug, and J. E. Sipe, "Bragg grating solitons," *Phys. Rev. Lett.* **76**, 1627 (1996).

[33] S. J. Carter, P. D. Drummond, M. D. Reid, and R. M. Shelby, "Squeezing of quantum solitons," *Phys. Rev. Lett.* **58**, 1841 (1987).

[34] P. D. Drummond and S. J. Carter, "Quantum-field theory of squeezing in solitons," *J. Opt. Soc. Am. B* **4**, 1565 (1987).

[35] S. J. Carter, P. D. Drummond, and R. M. Shelby, "Time dependence of quantum fluctuations in solitons," *Opt. Lett.* **14**, 373 (1989).

[36] Y. Lai and H. A. Haus, "Quantum theory of solitons in optical fibers. I. Time-dependent Hartree approximation," *Phys. Rev. A.* **40**, 844 (1989).

[37] Y. Lai and H. A. Haus, "Quantum theory of solitons in optical fibers. II. Exact solution," *Phys. Rev. A* **40**, 854 (1989).

[38] Y. Lai and H. A. Haus, "Quantum theory of self-induced transparency solitons: A linearization approach," *Phys. Rev. A* **42**, 2925 (1990).

[39] V.V. Konotop and M. Salerno, "Modulational instability in Bose-Einstein condensates in optical lattices," *Phys. Rev. A* **65**, 021602(R) (2002).

[40] P. J. Y. Louis, E. A. Ostrovskaya, C. M. Savage, and Yu. S. Kivshar, "Bose-Einstein condensates in optical lattices: Band-gap structure and solitons," *Phys. Rev. A* **67**, 013602 (2003).

[41] V. Ahufinger, A. Sanpera, P. Pedri, L. Santos, and M. Lewenstein, "Creation and mobility of discrete solitons in Bose-Einstein condensates," *Phys. Rev. A* **69**, 053604 (2004).

[42] J. W. Fleischer, T. Carmon, and M. Segev, "Observation of Discrete Solitons in Optically Induced Real Time Waveguide Arrays," *Phys. Rev. Lett.* **90**, 023902 (2003).

[43] D. Neshev, E. A. Ostrovshaya, Yu. S. Kivshar, and W. Krolikowski, "Spatial solitons in optically induced gratings," *Opt. Lett.* **28**, 710 (2003).

[44] J. W. Fleischer, M. Segev, N. K. Efremidis, and D. N. Christodoulides, "Observation of two-dimensional discrete solitons in optically induced nonlinear photonic lattices," *Nature (London)* **422**, 147 (2003).

[45] L. Khaykovich F. Schreck, G. Ferrari, T. Bourdel, J. Cubizolles, L. D. Carr, Y. Castin, and C. Salomon, "Formation of a matter-wave bright soliton," *Science* **296**, 1290 (2002).

[46] K. E. Strecker, G. B. Partridge, A.G. Truscott, and R.G. Hulet, "Formation and propagation of matter-wave soliton trains," *Nature (London)* **417**, 150 (2002).

[47] Z. Cheng and G. Kurizki, "Theory of one-dimensional quantum gap solitons," *Phys. Rev. A* **54**, 3576 (1996).

[48] H. A. Haus and Y. Lai, "Quantum theory of soliton squeezing: a linearized approach," *J. Opt. Soc. Am. B* **7**, 386 (1990).

[49] S. R. Friberg, S. Machida, M. J. Werner, A. Levanon, and T. Mukai, "Observation of optical soliton photon-number squeezing," *Phys. Rev. Lett.* **77**, 3775 (1996).

[50] T. Opatrný, N. Korolkova, and G. Leuchs, "Mode structure and photon number correlations in squeezed quantum pulses," *Phys. Rev. A* **66**, 053813 (2002).

[51] G. Lenz and B. J. Eggleton, "Adiabatic Bragg soliton compression in nonuniform grating structures," *J. Opt. Soc. Am. B* **15**, 2979 (1998).

[52] M. J. Werner, "Quantum soliton generation using an interferometer," *Phys. Rev. Lett.* **81**, 4132 (1998).

[53] H. Pu and P. Meystre, "Creating Macroscopic Atomic Einstein-Podolsky-Rosen States from Bose-Einstein Condensates," *Phys. Rev. Lett.* **85**, 3987 (2000)

[54] L.-M. Duan, A. Sorensen, J. I. Cirac, and P. Zoller, "Squeezing and Entanglement of Atomic Beams," *Phys. Rev. Lett.* **85**, 3991 (2000).

[55] C. Orzel, A. K. Tuchman, M. L. Fenselau, M. Yasuda, and M. A. Kasevich, "Squeezed states in a Bose-Einstein condensate," *Science* **291**, 2386 (2001).

[56] A. Sørensen L.-M. Duan, J. I. Cirac, P. Zoller, "Many-particle entanglement with Bose-Einstein condensates," *Nature (London)* **409**, 63 (2001).

[57] J. M. Vogels, K. Xu, and W. Ketterle, "Generation of macroscopic pair-correlated atomic beams by four-wave mixing in Bose-Einstein condensates," *Phys. Rev. Lett.* **89**, 020401 (2002).

[58] S. Spälter N. Korolkova, F. König, A. Sizmann, and G. Leuchs, "Observation of multimode quantum correlations in fiber optical solitons," *Phys. Rev. Lett.* **81**, 786 (1998)

[59] A. Sizmann and G. Leuch, "The optical Kerr effect and quantum optics in fibers," in *Prog. Opt.* **34**, 373 edited by E. Wolf (Elsevier, Amsterdam, 1999).

[60] S.A. Haine and J.J. Hope, "Mode selectivity and stability of continuously pumped atom lasers," *Phys. Rev. A*, 68, 23607 (2003).

[61] L. O. Baksmaty, W. Zhang, N. P. Bigelow, and P. Meystre, "Effective-mass analysis of Bose-Einstein condensates in optical lattices: Stabilization and levitation," *Phys. Rev. A*, **67**, 043605 (2003)

[62] M. Rosenbluh and R. Shelby, "Squeezed optical solitons," *Phys. Rev. Lett.* **66**, 153 (1991).

[63] K. Bergman and H. A. Haus, "Squeezing in fibers with optical pulses," *Opt. Lett.* **16**, 663 (1991).

[64] R.-K. Lee and Y. Lai, "Amplitude-squeezed fiber-Bragg-grating solitons," *Phys. Rev. A* **69**, 021801(R) (2004).

[65] F. König, M. A. Zielonka, and A. Sizmann, "Transient photon-number correlations of interacting solitons," *Phys. Rev. A* **66**, 013812 (2002).

[66] Ch. Silberhorn, P. K. Lam, O. Weib, F. König, N. Korolkova, and G. Leuchs, "Generation of continuous variable Einstein-Podolsky-Rosen entanglement via the kerr nonlinearity in an optical fiber," *Phys. Rev. Lett.* **86**, 4267 (2001).

[67] Ch. Silberhorn, N. Korolkova, and G. Leuchs, "Quantum Key Distribution with Bright Entangled Beams," *Phys. Rev. Lett.* **88**, 167902 (2002).

[68] O. Glöckl, S. Lorenz, C. Marquardt, J. Heersink, M. Brownnutt, C. Silberhorn, Q. Pan, P. van Loock, N. Korolkova, and G. Leuchs, "Experiment towards continuous-variable entanglement swapping: Highly correlated four-partite quantum state ," *Phys. Rev. A* **68**, 012319 (2003).

[69] A. Furusawa, J. L. Sørensen, S. L. Braunstein, C. A. Fuchs, H. J. Kimble, and E. S. Polzik, "Unconditional quantum teleportation," *Science* **282**, 706 (1998).

[70] T. C. Ralph and P. K. Lam, "Teleportation with bright squeezed light," *Phys. Rev. Lett.* **81**, 5668 (1998).

[71] G. P. Agrawal, *"Nonlinear Fiber Optics,"* (Academic, San Diego, 1995).

[72] B. A. Malomed, "Bound solitons in the nonlinear SchrodingerVGinzburg-Landau equation," *Phys. Rev. A* **44**, 6954, (1991).

[73] I. M. Uzunov, R. Muschall, M. Gölles, F. Lederer, and S. Wabnitz, "Effect of nonlinear gain and filtering on soliton interaction," *Opt. Comm.* **118**, 577 (1995).

[74] N. N. Akhmediev, V. V. Afanasjev, and J. M. Soto-Crespo, "Singularities and special soliton solutions of the cubic-quintic complex Ginzburg-Landau equation," *Phys. Rev. E* **53**, 1190 (1996).

[75] N. N. Akhmediev, A. Ankiewicz, and J. M. Soto-Crespo, "Multisoliton solutions of the complex Ginzburg-Landau equation," *Phys. Rev. Lett.* **79**, 4047 (1997).

[76] J. M. Soto-Crespo, N. N. Akhmediev, V. V. Afanasjev, and S. Wabnitz, "Pulse solutions of the cubic-quintic complex Ginzburg-Landau equation in the case of normal dispersion," *Phys. Rev. E* **55**, 4783 (1997).

[77] V. V. Afanasjev, B. A. Malomed, and P. L. Chu, "Stability of bound states of pulses in the Ginzburg-Landau equations," *Phys. Rev. E* **56**, 6020 (1997).

[78] N. N. Akhmediev, A. Ankiewicz, and J. M. Soto-Crespo, "Stable soliton pairs in optical transmission lines and fiber lasers," *J. Opt. Soc. Am. B* **15**, 515 (1998).

[79] M. Haelterman, A. P. Sheppard, and A. W. Snyder, "Bound-vector solitary waves in isotropic nonlinear dispersive media," *Opt. Lett.* **18**, 1406 (1993).

[80] D. J. Kaup, B. A. Malomed, and R. S. Tasgal, "Internal dynamics of a vector soliton in a nonlinear optical fiber," *Phys. Rev. E* **48**, 3049, (1993).

[81] B. A. Malomed and R. S. Tasgal, "Internal vibrations of a vector soliton in the coupled nonlinear Schrodinger equations," *Phys. Rev. E* **58**, 2564 (1998).

[82] D. Y. Tang, W. S. Man, H. Y. Tam, and P. D. Drummond, "Observation of bound states of solitons in a passively mode-locked fiber laser," *Phys. Rev. A* **64**, 033814 (2001).

[83] N. H. Seong and Dug Y. Kim, "Experimental observation of stable bound solitons in a figure-eight fiber laser," *Opt. Lett.* **27**, 1321 (2002).

[84] P. Grelu, F. Belhache, F. Gutty, and J. M. Soto-Crespo, " Relative phase locking of pulses in a passively mode-locked fiber laser," *J. Opt. Soc. Am. B* **20**, 863 (2003).

[85] G. Steinmeyer and F. Mitschke, "Longitudinal structure formation in a nonlinear resonator," *Appl. Phys. B* **62**, 367 (1996).

[86] M. Salerno, "Macroscopic quantum bound states of Bose Einstein condensates in optical lattices," arXiv:cond-mat/0311630.

[87] S. R. Fridberg, Takaaki Mukai, and Susumu Machida, "Dual Quantum Nondemolition Measurements via Successive Soliton Collisions," *Phys. Rev. Lett.* **84**, 59 (2000).

[88] B. A. Malomed, *Variational methods in nonlinear fiber optics and related fields,"* in *Progress in Optics*, **43**, 71 edited by E. Wolf (Elsevier, Amsterdam, 2002).

[89] B.A. Malomed, A.I. Maimistov, and A. Desyatnikov, " potential of incoherent attraction between multidimensional solitons," *Phys. Lett. A* **254**, 179 (1999).

[90] R.-K. Lee, Y. Lai, and B. A. Malomed, "Quantum correlations in bound-soliton pairs and trains in fiber lasers," *Phys. Rev. A* **70**, xxxxxx (2004); quant-ph/0408175.

[91] R.-K. Lee and Y. Lai, "Fluorescence squeezing spectra near a photonic bandgap," *J. Opt. B* **6**, S715 (2004).

[92] R.-K. Lee and Y. Lai, "Quantum theory of fiber Bragg grating solitons," *J. Opt. B* **6**, S638 (2004).

[93] R.-K. Lee, E. A. Ostrovskaya, Yu. S. Kivshar, and Y. Lai, "Squeezing and entanglement of matter-wave gap solitons," submitted for publication; quant-ph/0412036.

[94] R.-K. Lee, Y. Lai, and B. A. Malomed, "Generation of photon-number entangled soliton pairs through interactions," *Phys. Rev. A* **71**, xxxxxx (2005); quant-ph/0405138.